Radiation-Hardened Circuitry Using Mask-Programmable Analog Arrays: Report 3

C. L. Britton
J. Shelton
M. N. Ericson
M. Bobrek
B. Blalock

March 2015

OAK RIDGE NATIONAL LABORATORY
MANAGED BY UT-BATTELLE FOR THE US DEPARTMENT OF ENERGY

CONTENTS

LIST OF FIGURES

Figures   **Page**

LIST OF TABLES

ACRONYMS

ADC	analog-digital converter
ASIC	application-specific integrated circuit
csv	comma-separated value
DN	digital number
FPGA	field-programmable gate array
FMI	Frequency Management International
G-M	Geiger-Mueller
IC	integrated circuit
NEET	Nuclear Energy Enabling Technologies
PC	personal computer
PCB	printed circuit board
TID	total ionizing dose
UART	universal asynchronous receiver/transmitter
VCA	Via-Configurable Array

ABSTRACT

As the recent accident at Fukushima Daiichi so vividly demonstrated, telerobotic technologies capable of withstanding the conditions encountered in high-radiation environments need to be readily available to enable operations, repair, and recovery under severe accident scenarios when human entry is extremely dangerous or not possible. Telerobotic technologies have undergone revolutionary improvement during the past few decades and may enable remote operation in high-dose-rate environments. However, in many cases these technologies cannot be employed in nuclear power environments because of the radiation sensitivity of the electronic components and the organic insulator materials currently in use.

This is a report on the status of activities involving Task III of the Nuclear Energy Enabling Technologies 2 project, "Radiation Hardened Circuitry Using Mask-Programmable Analog Arrays" [1]. Evaluation of the performance of the system for both pre- and post-irradiation as well as operation at elevated temperature was performed. In this context, the *system* in this report is a collection of precommercial radiation-hardened (rad-hard) electronic components (on a rad-hard board) that is intended to process signals from environmental sensors measuring the ambient conditions of nuclear reactor. Detailed performance of the system was documented to ensure that the design meets requirements prior to any extended evaluation.

A suite of tests developed during Task III allows evaluation before and after irradiation and during exposure to elevated temperature. The radiation exposure facility, a laboratory at Arizona State University, was selected in the early phase of the project. Radiation exposure consists of total integrated dose above 200 kRad with several intermediate doses during the test. With a target of 30 kRad/h, dose rates were selected in various ranges determined by the radiation exposure facility .

Many samples of the precommercial devices to be used had been tested in previous projects to doses of at least 300 kRad and to temperatures up to 125°C. Therefore, complete systems [2, 3]were tested for performance at intermediate doses during this task. Extended temperature testing has been performed up to the limit of the commercial sensors (typically 125°C). The suite of tests have been performed at each set of conditions (often called a test point), which consists of operational testing of three basic measurement functions (signal conditioning, signal processing, and control) plus electronic functional testing (e.g., power dissipation, voltage offset changes, noise variations).

1. PROJECT STATUS

Currently, activities for Task III are on schedule. The published schedule shown in the project plan [1] states that pre- and postradiation validation, as well as system performance as a function of temperature, should be completed by the middle of the third quarter of FY 2015. Presently, complete system calibrations have been finished for temperature, pressure, and gamma radiation counts for all five systems. In addition, data—as a function of total integrated dose (TID) radiation—have been acquired for all three important nuclear reactor ambient parameters, with satisfactory results. The personal computer-based LabVIEW data-acquisition software was modified (1) to utilize the system-calibration coefficients and to convert raw digital data into a useful display of all three parameters of importance continuously or at a certain time interval specified by the user and (2) to record the raw data in a local Excel file for further examination.

2. TEST-SUITE DEVELOPMENT

The development of a test to extract relevant and accurate results from a system is vital to a project's integrity, documentation, and presentation. The data acquisition system based on rad-hard mask-programmable analog arrays, outlined in Fig. 1, requires a suite of tests to capture complete functionality and performance data in extreme environments such as those found in monitoring and disaster scenarios developed for nuclear reactor operations. These environments are capable of wide temperature and pressure ranges as well as high-dose-rate radiation. The suite of tests must encompass all extremes of which these environments are capable. This section illustrates the setup for those tests using color-coded interconnects consistent with Fig. 1 and provides detailed descriptions of each.
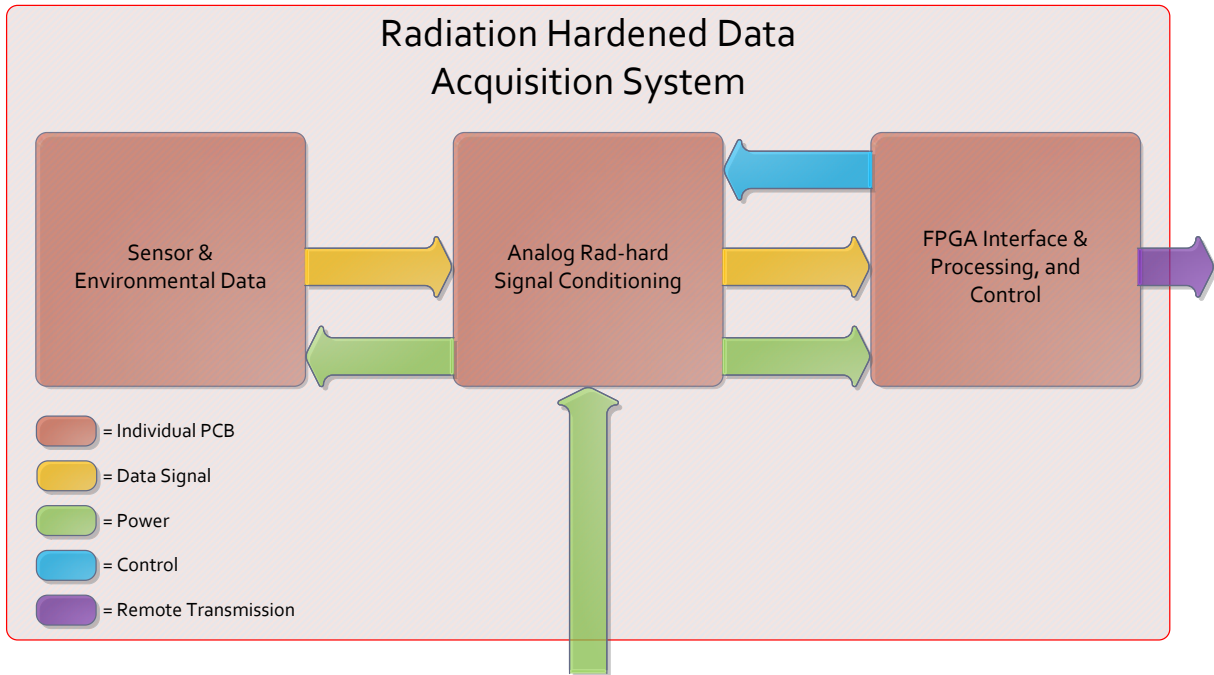
Fig. 1. System functional description.

2.1 TEMPERATURE CALIBRATION TEST SETUP

Within potentially harsh radiation environments such as nuclear reactor sites, ambient temperature can be a significant parameter for monitoring normal and stable reactor operating conditions and for detecting early signs of nuclear disaster situations. This is particularly true for pressurized-water reactors. As a result, accurate and frequent temperature measurements are necessary. The data acquisition system is capable of measuring ambient temperature, but the performance of this measurement needs to be characterized.

The obvious way to complete this characterization is to set up the system for nearly normal operation, but with the sensor board inside an environmental chamber that can precisely control the temperature to which the board is exposed. The chamber is used to sweep the temperature across a wide range and to let the system report temperature data points along the way. By recording the temperature chamber reading at certain intervals, as well as the system temperature data, any error can be approximated and factored out. This is considered to be the system's temperature calibration. To ensure a stable and consistent temperature throughout the chamber—and to ensure that the sensor board has reached equilibrium

temperature—a period of time is allotted at each data point interval in which the chamber temperature setting is unchanged. Figure 2 illustrates this test setup, including the sensor board within the temperature chamber, appropriate interconnect between each printed circuit board (PCB), power supplies, and field-programmable gate array (FPGA) universal asynchronous receiver/transmitter (UART) interface to the end-user personal computer (PC). A voltmeter also is used to record the output voltage of the temperature sensor, which will provide insight into any nonlinearity that may be present.
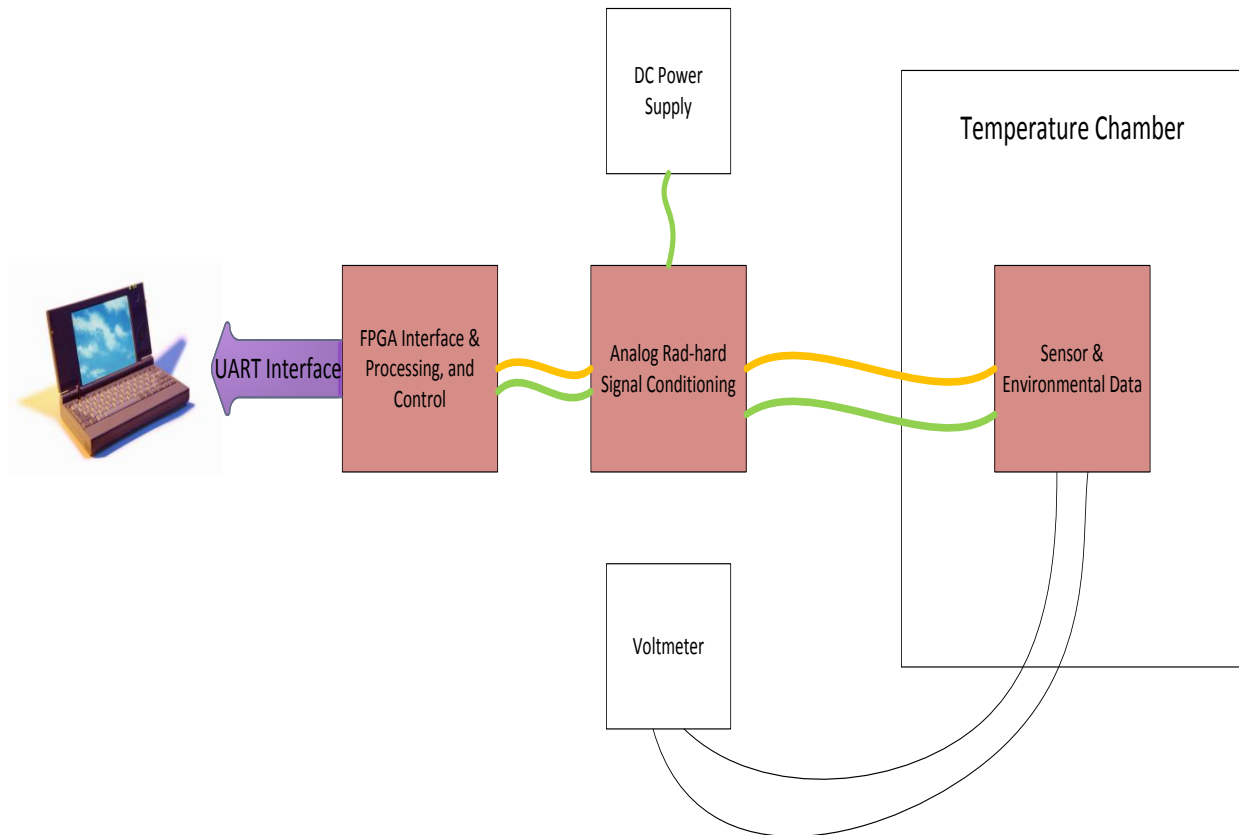
Fig. 2. System temperature calibration testing setup.

2.2   TEMPERATURE DRIFT CALIBRATION SETUP

Also of importance to characterizing the measurement performance of the data acquisition system is testing for any drift effects to due change in temperature of the rad-hard board. In realistic scenarios, it is likely that the entire system's temperature will change along with the temperature of the sensor board. Thus it is necessary to sweep the temperature of the sensor board and rad-hard board simultaneously. For the purposes of this project, the FPGA board is not required to operate at elevated temperatures, but future prototypes could incorporate this feature. An upper operational boundary of 125°C is achievable with silicon devices, so future implementations would utilize either a space-qualified FPGA or some version of a military-qualified controller device.

This test setup did not differ significantly from the one shown in Fig. 2, as the rad-hard board was moved into the temperature chamber along with the sensor board. However, it did require a slight change in wiring. Previously, only a single power and data cable were routed into the chamber. In this case, that power and data cable remains fully within in the chamber. An additional power cable was routed in to

power the system, and an additional data cable was routed in to provide a data path to the digital controller, which remains outside the chamber. Figure 3 portrays the temperature-drift test setup, along with the FPGA UART interface to the end-user PC. Once again, a voltmeter was used to document temperature sensor output voltage readings to assist in analyzing any nonlinearity that may be apparent from the system calibrations.
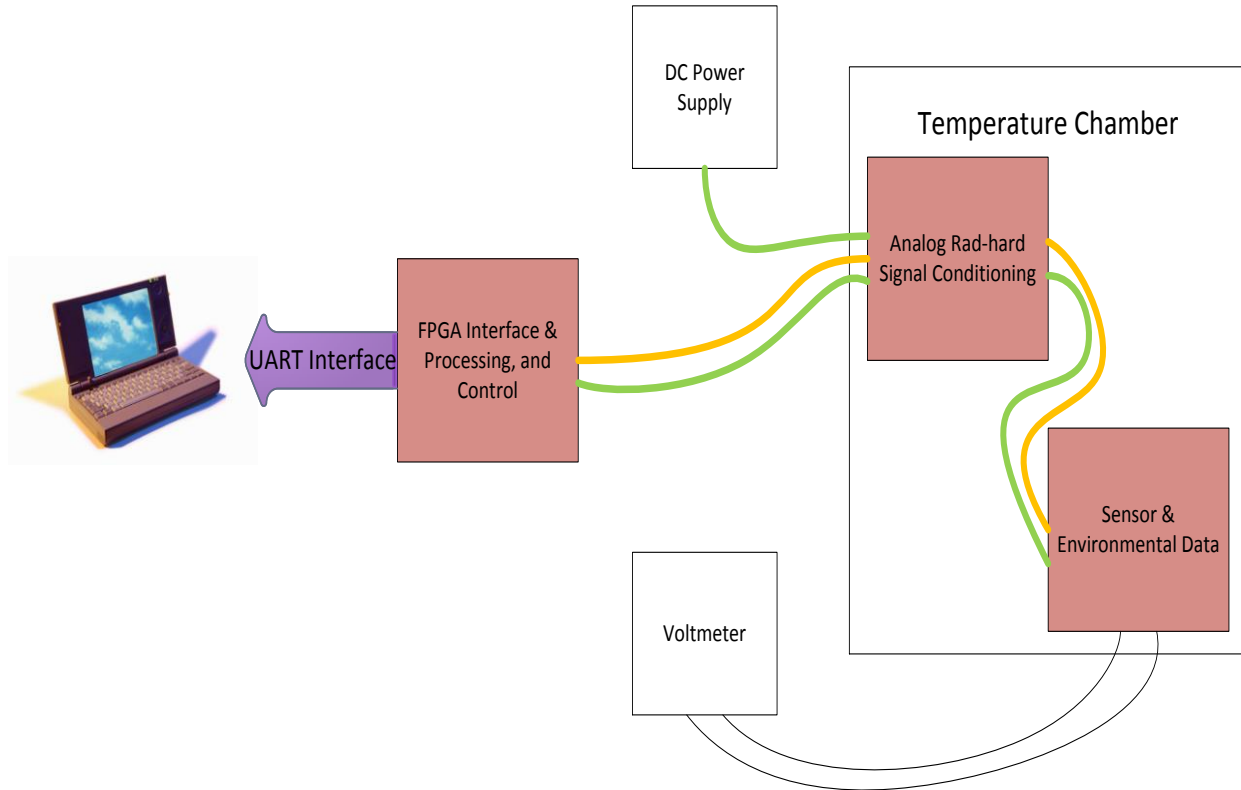
Fig. 3. System temperature drift calibration testing setup.

2.3 PRESSURE CALIBRATION TEST SETUP

Pressure and water levels are key parameters for boiling-water reactors, and pressure is another parameter that is monitored in reactor environments to reveal ideal or nonideal operating conditions and to indicate that unsafe conditions may be developing. For harsh environments, we want to measure pressure relative to normal atmospheric pressure, or gauge pressure, up to 2 atm (3 atm absolute). The pressure sensor on the data acquisition system is capable of measuring up to 30 psi relative pressure (45 psi absolute), which covers this range requirement but needs characterization to accurately report instantaneous ambient pressure data.

Creating a pressure condition in a test environment is different from creating a temperature condition because the pressure of interest typically is conveyed through some tube or pipe (e.g., from within a reactor building) instead of presenting an ambient condition to which the data acquisition system would be exposed. Hence the entire system need not be sealed in a pressure chamber for testing. The ASDX series Honeywell pressure sensor features an axial vented port, which can be easily pressure-sealed using a silicon tube at such relatively low pressure levels. Therefore, a pressure generator with a fine-tunable regulator is sufficient for sweeping across the specified pressure range in 2.5 psi increments. This allows normal operating condition setup of the data acquisition system for pressure calibration with only the addition of a pressure generator and tubing connected directly to the vented axial port of the pressure

4

sensor. This test can be executed much more quickly than the temperature test because pressure change and equilibrium are reached abruptly, and no time allotment between data points is needed. The pressure calibration test setup is shown in Fig. 4.
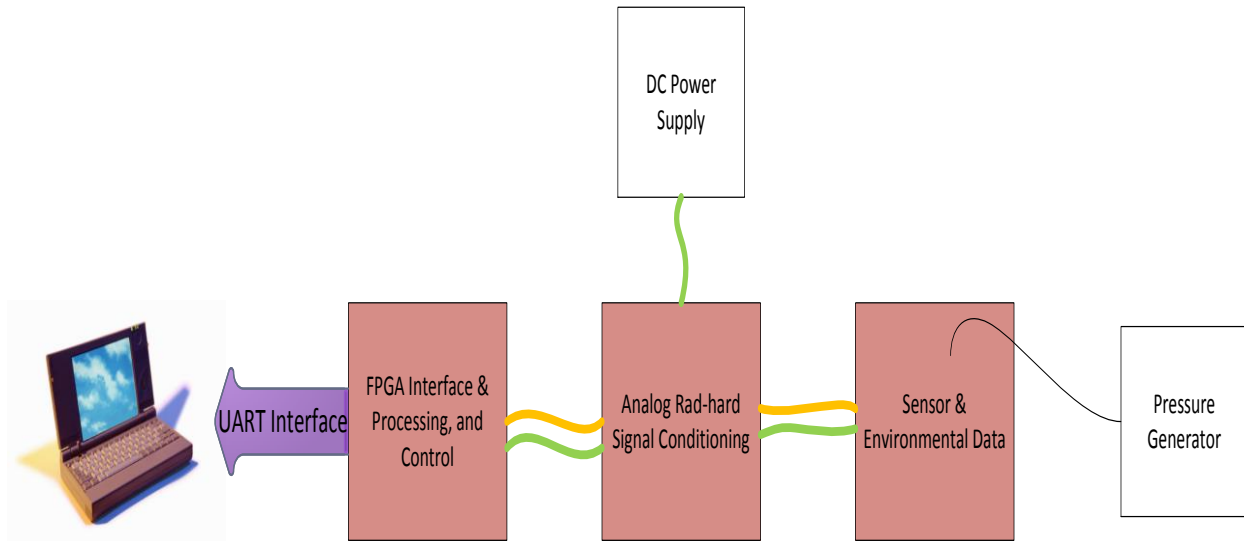
Fig. 4. System pressure calibration testing setup.

2.4   RADIATION TESTING SETUP

2.4.1   Site Selection

There are many parameters that categorize a radiation test site, including radiation source type, dose distribution, and dose rate. All of these parameters can vary greatly, depending on the exposure facility. The application often determines which configuration would be best for obtaining realistic, useful system radiation-tolerance data. For the data acquisition system in particular, we are interested in TID radiation potentially up to 300 kRad at a target dose rate of 30 kRad/h. In addition, a 360° dose distribution also is useful for this system due to the large area required (approximately 4.5" X 6")of the rad-hard board to mount all of the necessary application-specific integrated circuits (ASICs). It will help provide an even distribution of radiation dose across the entire board area and will ensure proper radiation exposure to all circuit elements designed for radiation hardness—as would be expected during an immersive exposure to high-energy emissions characteristic of reactor accident scenarios.

TID radiation in the environments of interest comes primarily from gamma rays or high-energy photons. The most common and cost-efficient radiation source that fits these specifications by nuclear decay (a much more convenient photon source than a high-energy X-ray generator) is cobalt-60, which has photopeaks at 1.186 and 1.348 MeV. Numerous radiation exposure facilities house cobalt-60 sources, but all specifications must be met. Many facilities were considered, including options on site at Oak Ridge National Laboratory. The conclusion was made that a laboratory at Arizona State University, under the direction of Dr. Keith Holbert, was the best fit for our application. This lab is equipped with a Gammacell 220, which is a 360º distributing cobalt-60 source. This cell provides an isotropic dose (see Fig. 5) that produces a dose rate of 28.62 kRad/h during the time period of radiation testing. A chamber that contains the devices to be irradiated is lowered into the pool with a path out the chamber's roof for cabling. Dr. Keith Holbert also is a primary investigator for another project under Nuclear Energy Enabling Technologies (NEET) 2 (project CT-14ID070402).
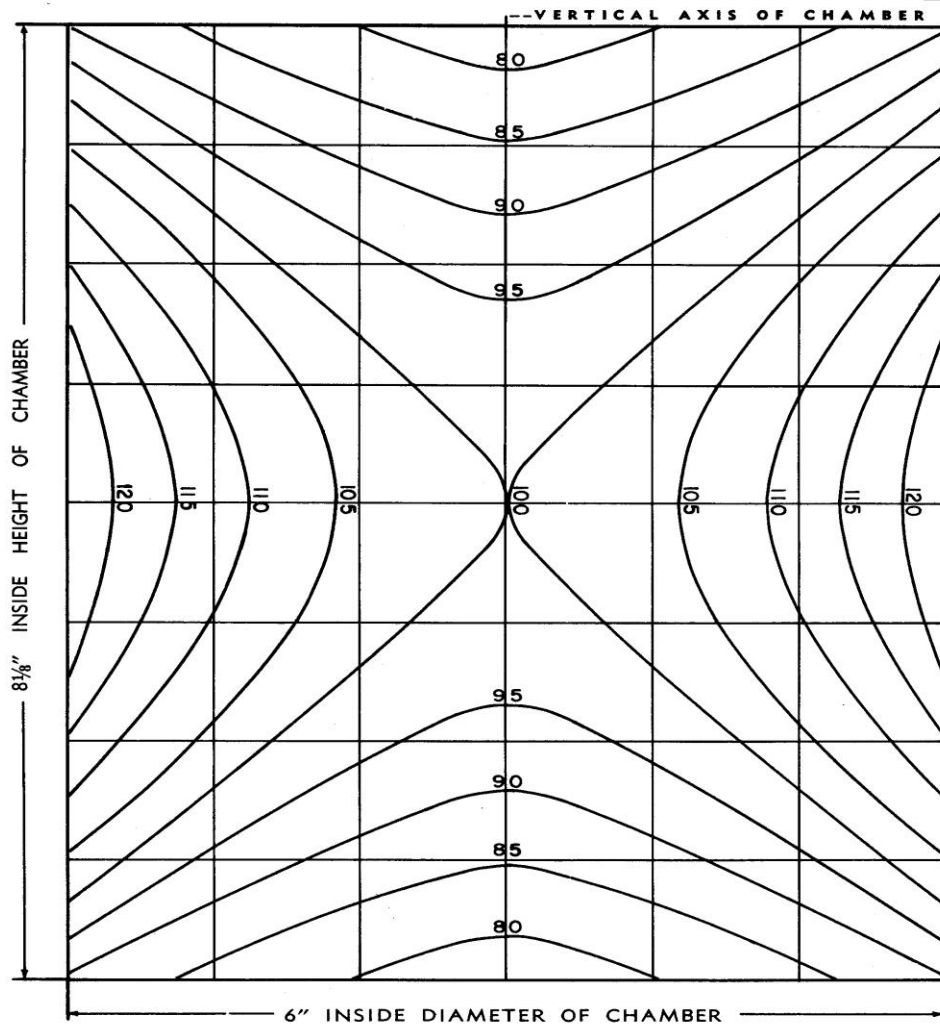
Fig. 5. Gammacell 220 isodose curves.

2.4.2   Test Setup

Radiation detection is the key parameter in identifying a nuclear reactor disaster scenario. Radiation can and will escape reactor containment before an event-related change to ambient temperature or pressure is measured. A test setup that exposes the proper boards to gamma radiation and protects the vulnerable components from harmful dose rates, all while allowing ambient parameter and power-consumption data to be taken, is crucial to the accuracy and prolonged operation of the entire system.

Because only the rad-hard board will be lowered in the radiation pool at the test facility, multiple cables and wiring will need to be irradiated as well. This includes the power cable from the voltage supply, data

6

and power cables to the sensor board, and data and power cables to the FPGA controller board. These cables will need to be recycled after each system is irradiated because the polyvinyl chloride insulating material will begin to deteriorate at high TID. A final rad-hard system used on a robot would be constructed with shielded cables or with mineral-insulated cables. Also, since the Geiger-Mueller (G-M) tube will be in use to monitor any background radiation, the sensor board will need to be placed in a high-voltage protection box to safeguard against any incidental contact with the existing voltage. In addition, power consumption is an important parameter that is susceptible to radiation effects if not properly protected or otherwise hardened, so system voltage and current are measured for the duration of the test. This is done by simply connecting a voltmeter across the terminals of the voltage supply as well as an ammeter in series with the positive referenced current supply. Due to the immobility of direct-current power supplies, a battery better suits the application of rad-hard data acquisition for nuclear reactor monitoring compared to a wired system; thus, a 9.6 V nickel-metal hydride battery is used as the power supply during radiation testing. Figure 6 illustrates the radiation testing setup.
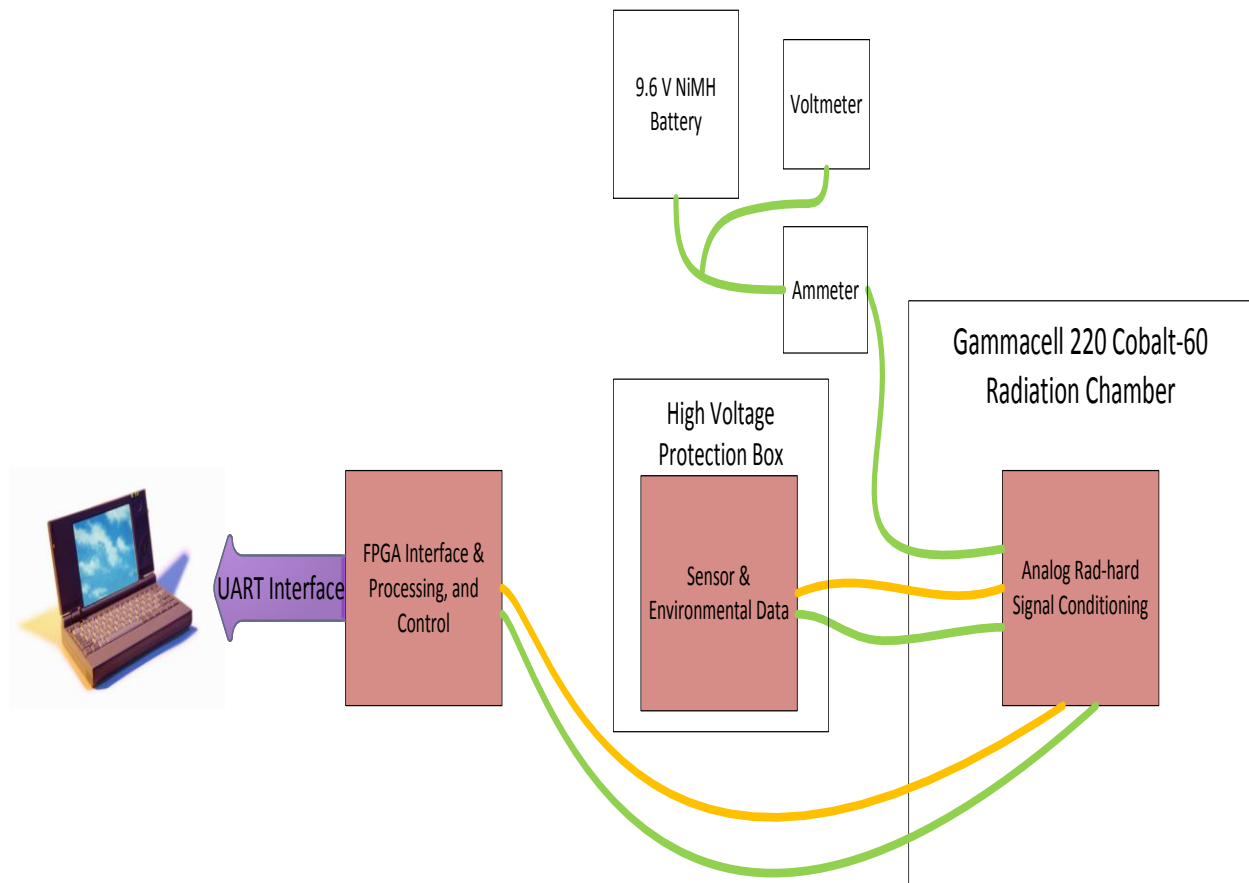
Fig. 6. System radiation testing setup.

2.5   LABVIEW INTERFACE SOFTWARE CODE DEVELOPMENT

The previous version of the LabVIEW interface program collected data from the Nexys 3 board programming and simply displayed the value of the data. It transmitted the selected UART command and displayed the return value of the requested command. It also configured the COM port on the computer to the appropriate settings. That version was sufficient to gather data during calibration testing but was unable to use the curve coefficients found during calibration to convert the raw digital data back to useful ambient data. The final goal of the data acquisition system is to provide intelligible data to the end users

7

so that they can assess a reactor environment operating condition. Modifications to the LabVIEW software were necessary to allow temperature and pressure to be directly displayed. Mathematical functions such as multiplication, division, addition, subtraction, square roots, and squaring were implemented to enable solving of equations. These equations differed between the temperature and pressure calibration coefficients because the temperature curves use a polynomial fit (see Sect. 3.1, Table 1) and pressure curves use a linear fit (see Sect. 3.2, Table 2). In addition, because five complete systems were calibrated for both temperature and pressure, an array subset function was implemented to allow users to select which system is being tested and hence which set of calibration coefficients to use.

The converted data also needed to be actively plotted so users can visually discern the operating conditions of the system's ambient environment as a function of time. This required using LabVIEW's graphing palette and array builder to construct an array of x and y coordinate points, x being time and y being ambient data. This was done for all three sets of ambient data: temperature, pressure, and gamma radiation events. The temperature and pressure displays need be instantaneous, so a simple plotting of the x and y coordinate points would suffice. The gamma event display, however, should be a dose rate measurement. This means that the y data are normalized to number of counts per second. This conversion requires calculating the time elapsed between each data point and dividing the number of counts that occurred within that cycle by the measured time. Then a true dose rate with units of counts per second can be used to create an array that can be plotted by LabVIEW's graphing block. All of these graphs, along with all other functionality implanted within the LabVIEW software used for final testing, are shown in Fig. 7.

Third, all of the data in the arrays used for visual graphing not only need to be displayed continuously to the end user for active monitoring, but also should be stored as pure data into a local file for later examination. For each system tested, a separate location can be assigned to write the data into a specific comma-separated value (csv) file as the arrays are updated. LabVIEW features a block called "write to spreadsheet" that executes this functionality with options such as append file, transpose data, and data formatting for complete customization of the csv file in which the data are written. Completely developed LabVIEW software visual code for top-level and sub-VI interfacing can be seen in Appendix A.
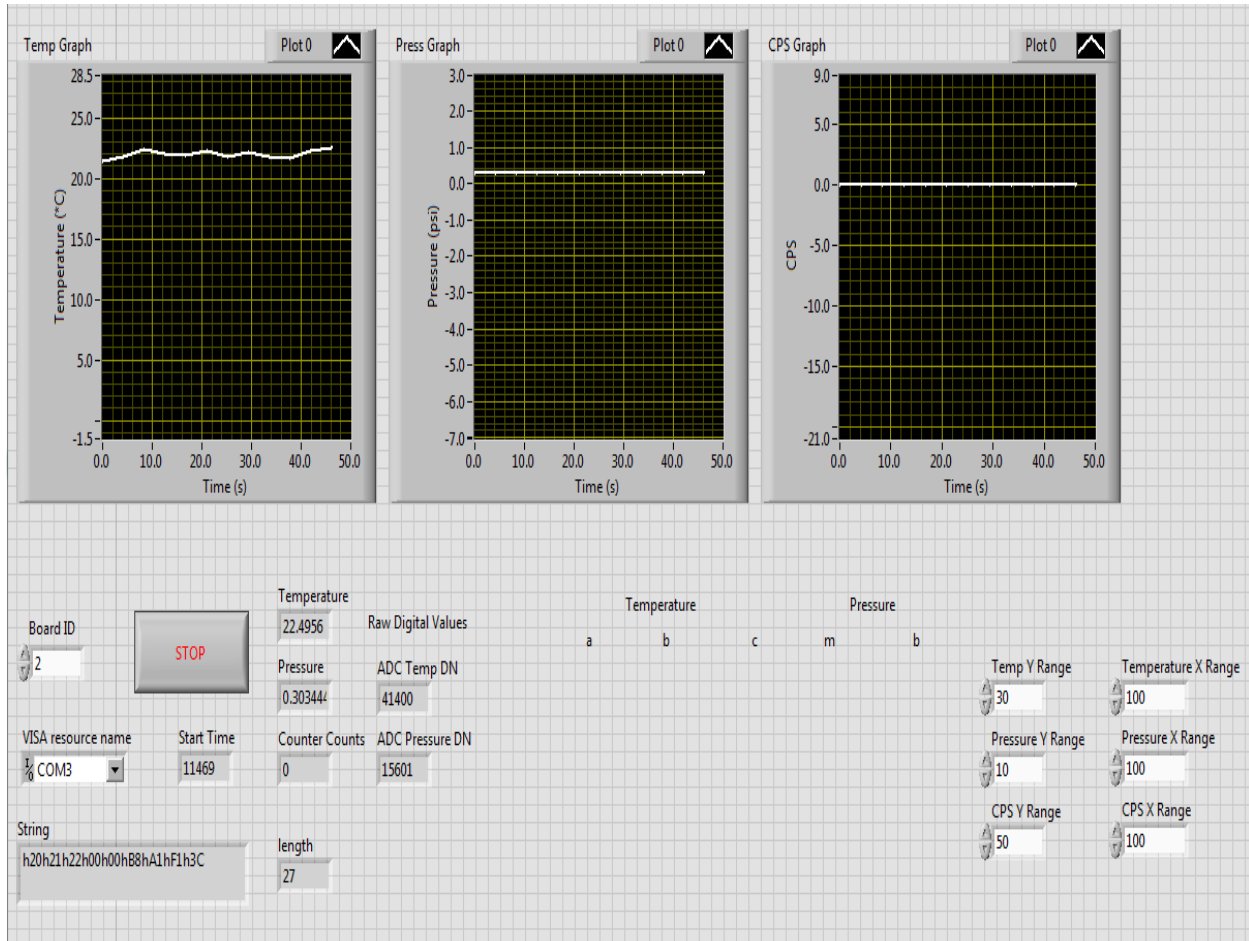
Fig. 7. LabVIEW interface software used for calibration and radiation testing.

3. PREIRRADIATION CALIBRATION TESTING

Due to the extremely high cost of rad-hard parts such as sensors and FPGAs, the rad-hard data acquisition system for Task III of the NEET 2 project was partitioned across three board designs (see Fig. 1). One board houses all the necessary rad-hard integrated circuits (ICs), such as the Triad Via-Configurable Array (VCA) [4], the Frequency Management International (FMI) frequency synthesizer [5], and voltage regulators. Commercial sensors could be mounted on one of the remaining two boards, and a digital controller could be mounted on the other. Because the system is spread across three boards, the required cabling and longer wire traces create parasitic power and signal drains that induce some variations between individual systems. Inherently, there will be system-to-system variations regardless of board partitioning because the IC fabrication process, although precise, is not perfect, and silicon substrate variations from chip to chip are inevitable. Although these variations at the chip and board level typically are small, they need to be accounted for in order to preserve the integrity of the data acquisition process.

An easy way to mitigate variations is to calibrate each system individually. This includes recording the final system output digital number (DN) of each data path for a specific known input value. The input value is swept across the entire range of possible inputs at a certain interval, and data are recorded at each step. If enough data points are taken, the final output DN then can be plotted vs the input range to portray each system's specific output value curve for the selected input range. Each curve is fitted with an

9

equation, and thus output DNs can be mapped back to input ambient environmental data precisely for each system for easy display to the end user. Curve fitting is performed empirically by selecting the type of curve that best approximates the system's calibration data, which is quantified with a coefficient of determination, or r-squared, value. An r-squared value always falls between 0 and 1. A higher value denotes a better fit of the selected curve type to the measured data than a lower one. After a curve type is selected, the coefficients of the equation describing that curve, or trendline, can be extracted and used to directly convert digital outputs to proper inputs. The coefficients are static for each system and only need to be measured once. LabVIEW then uses them to automatically calculate the ambient input data based on the instantaneous system output.

3.1 TEMPERATURE CALIBRATION

The main focal points when analyzing calibration data are linearity and continuity. Linearity is important to ensure that the analog-to-digital converter (ADC) adds minimal distortion to the waveform being processed. Continuity is important to ensure that there are no inputs for which an output code is missing. The temperature ADC data in Fig. 8 show great linearity over the entire ADC input dynamic range at an r-squared value of 0.9998.
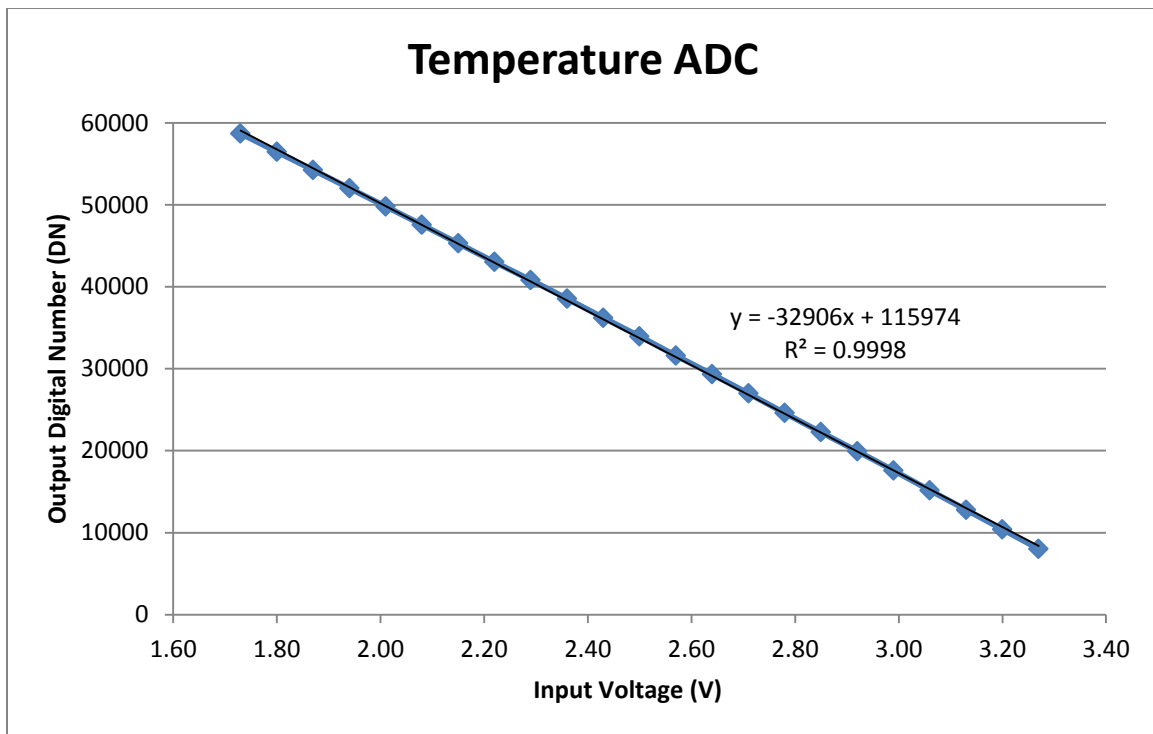
Fig. 8. Preliminary temperature ADC output DN vs input voltage.

Based on the excellent linearity of the circuits within the temperature data path on the rad-hard board, it can be stated that any nonlinearities in the overall system calibration measurement are attributed to the sensor board components. Some slight exponential behavior is expected from the sensor board. That behavior is due to the requirement of a current-to-voltage resistor on the output of the temperature sensor. It is well known that resistance changes to some degree as a function of temperature, even with high-precision, low-temperature-coefficient resistors. The sensor board is subjected to the most extreme temperature range of any board in order to model realistic operating conditions. Thus there will be an inevitable shift in the current-to-voltage resistance, resulting in a voltage shift as well, according to Ohm's Law.

10

Our published final project specification [1] requires five complete data acquisition systems be functional and tested across temperature and pressure. The result of temperature calibration for all five systems is shown in Figs. 9 through 13. The blue data points represent sweeping the temperature of the environmental chamber from –5°C to 70°C in 7.5°C increments with only the sensor board inside the chamber (Fig. 2). The rad-hard board and controller board are left outside the chamber in ambient room temperature.

Fig. 9. System 1 temperature output DN vs ambient temperature.

Fig. 10. System 2 temperature output DN vs ambient temperature.

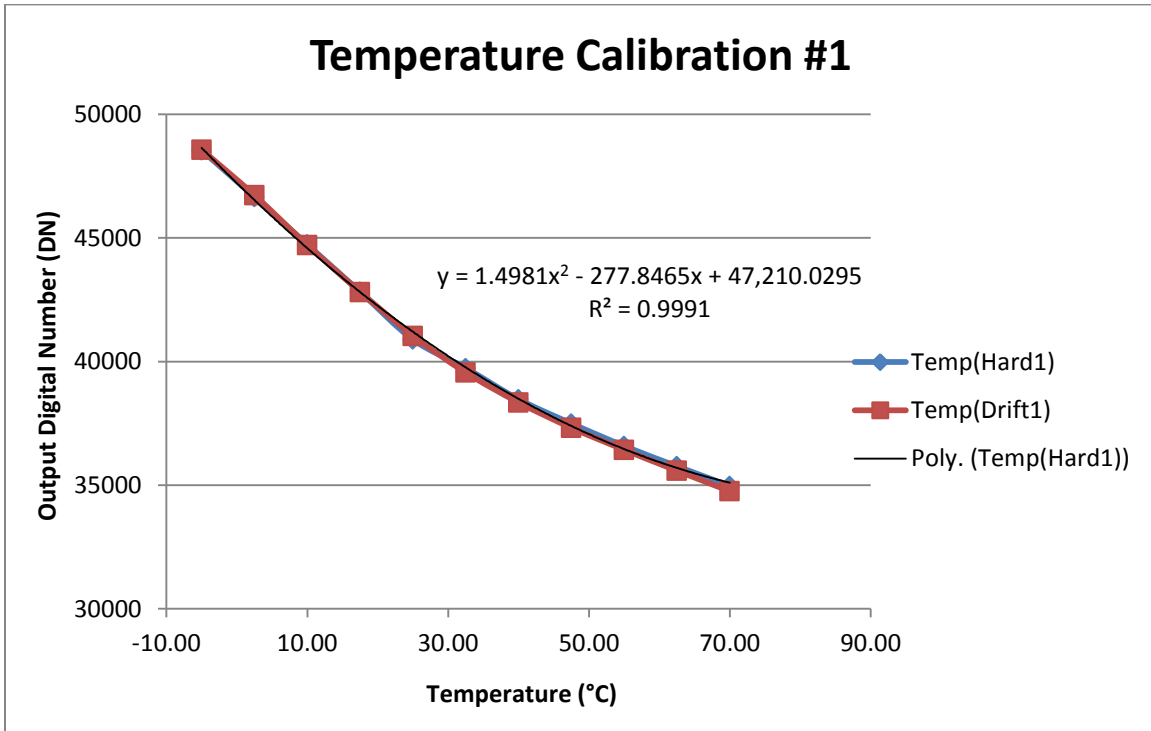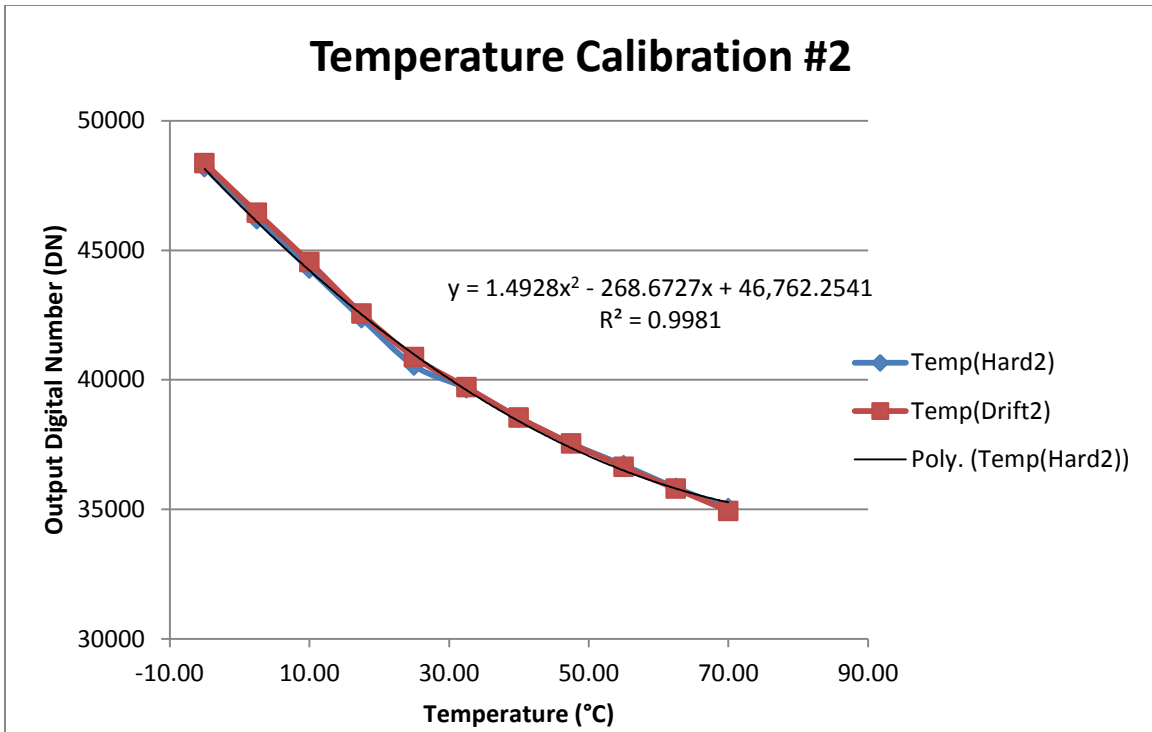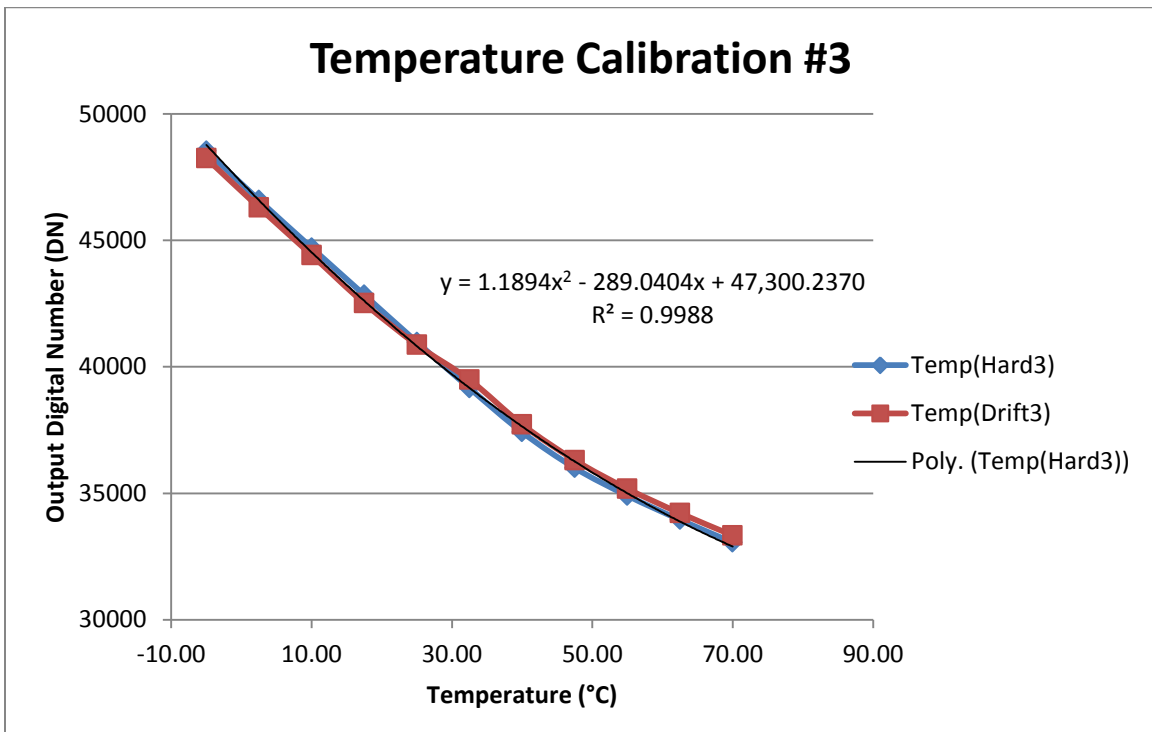**Fig. 11. System 3 temperature output DN vs ambient temperature.**
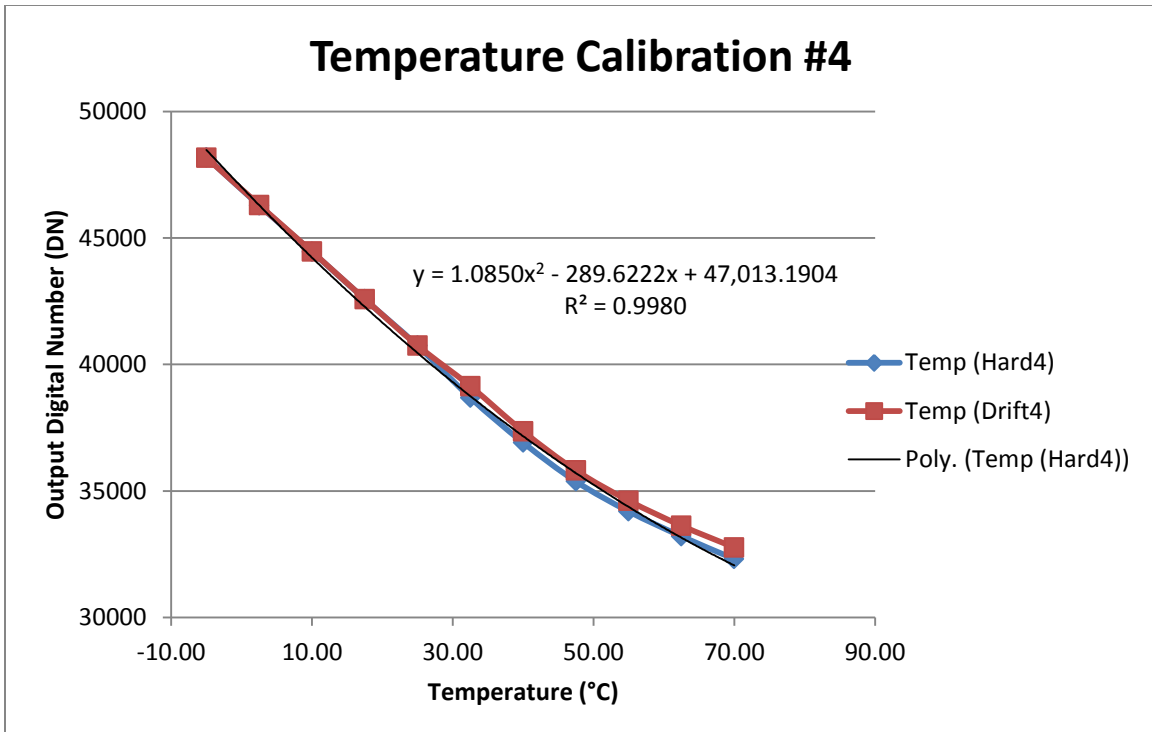
Fig. 12. System 4 temperature output DN vs ambient temperature.
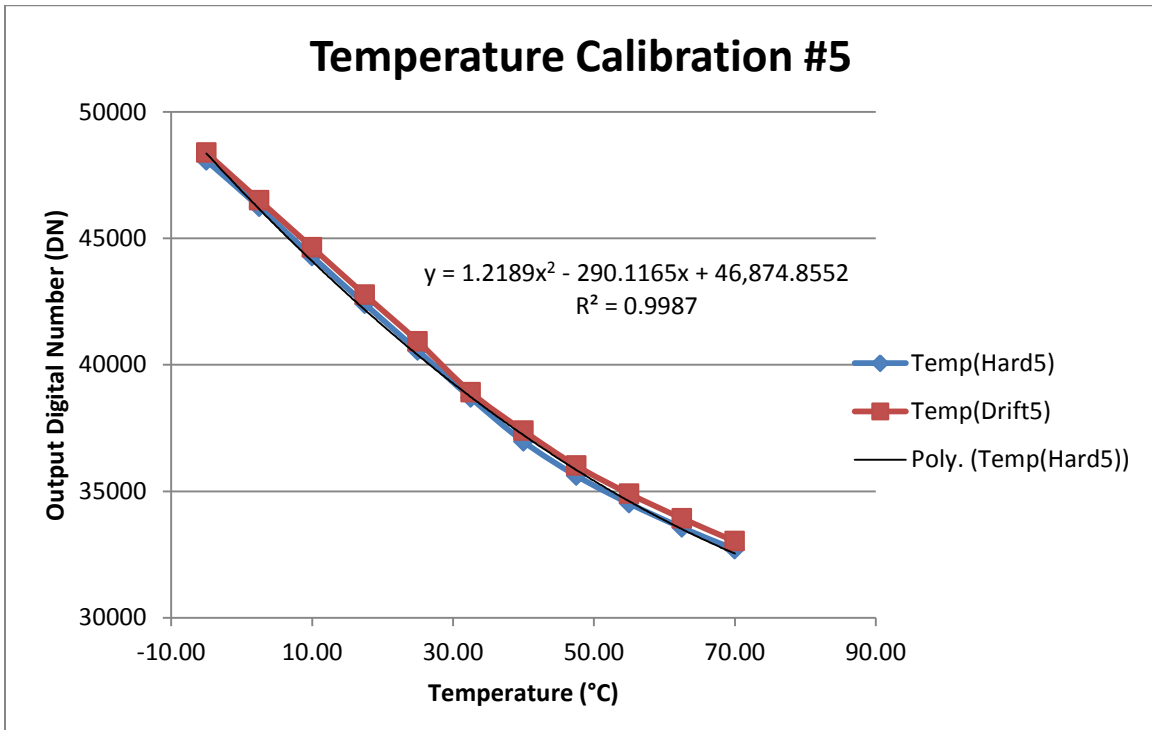

Fig. 13. System 5 temperature output DN vs ambient temperature.

As shown in the temperature calibration data, there is some apparent nonlinearity with an upward concavity. This behavior was expected and is in line with a concept known as resistance shifting: As the

chamber temperature decreases, the current-to-voltage resistance also decreases, resulting in a downward shift in voltage. This voltage reduction produces an increase in output DN, according to Fig. 8. Conversely, the opposite shift happens when chamber temperature increases. This behavior results in a concave-up curve of plotted DN vs temperature data.

Given the slight nonlinearity of the temperature calibration data, a linear trendline will not best approximate the curve. All five other regression types were examined, and a second-order polynomial approximation produced the highest r-squared value for all five systems. Table 1 summarizes the polynomial r-squared values and coefficients that are used by LabVIEW to convert output DNs to ambient data for each system.

Table 1. Summary of system temperature calibrations fit values and coefficients

| System	R-squared fit value	Coefficients (a, b, c)
1	0.9991	1.4981, –277.85, 47210.03
2	0.9981	1.4928, –268.67, 46762.25
3	0.9988	1.1894, –289.04, 47300.24
4	0.9980	1.0850, –289.62, 47013.19
5	0.9987	1.2189, –290.12, 46874.86

Complete system calibration data are also taken by sweeping the temperature of both the rad-hard circuitry and the sensor board in the environmental chamber so that any drift effects in the output DNs due to the wide temperature variation of the rad-hard circuitry can be analyzed and stated project objectives can be met (see Fig. 3). Results of this test will provide insight into the temperature performance capabilities of the system up to the final digitization of the pulse-width-modulated bit stream output of the sigma delta modulators.

As depicted by the red data points in Figs. 9 through 13, the drift of the output data as a function of temperature relative to the temperature calibration data (blue) is minimal. In fact, the data sets almost overlap exactly for all five systems. These outcomes are outstanding, considering all of the electrical biasing and functions that are temperature dependent and critical to the accuracy of the system, such as voltage references and current biases, the frequency synthesizer, and input node impedance within the temperature data path. Furthermore, the data verify the wide temperature capabilities of the Triad VCA and FMI frequency synthesizer ICs as well as all other ICs and designed circuitry present on the rad-hard board.

3.2   PRESSURE CALIBRATION

Just as with the temperature calibration, a measure of output pressure ADC DN while sweeping input voltage was performed to ensure that the signal conditioning and ADC circuits on the rad-hard board were linear with respect to input. These were preliminary tests to verify linearity of the rad-hard ADCs before moving on to complete system data calibration. Figure 14 shows the results of this input voltage sweep over the entire range of possible pressure sensor output voltages.

14
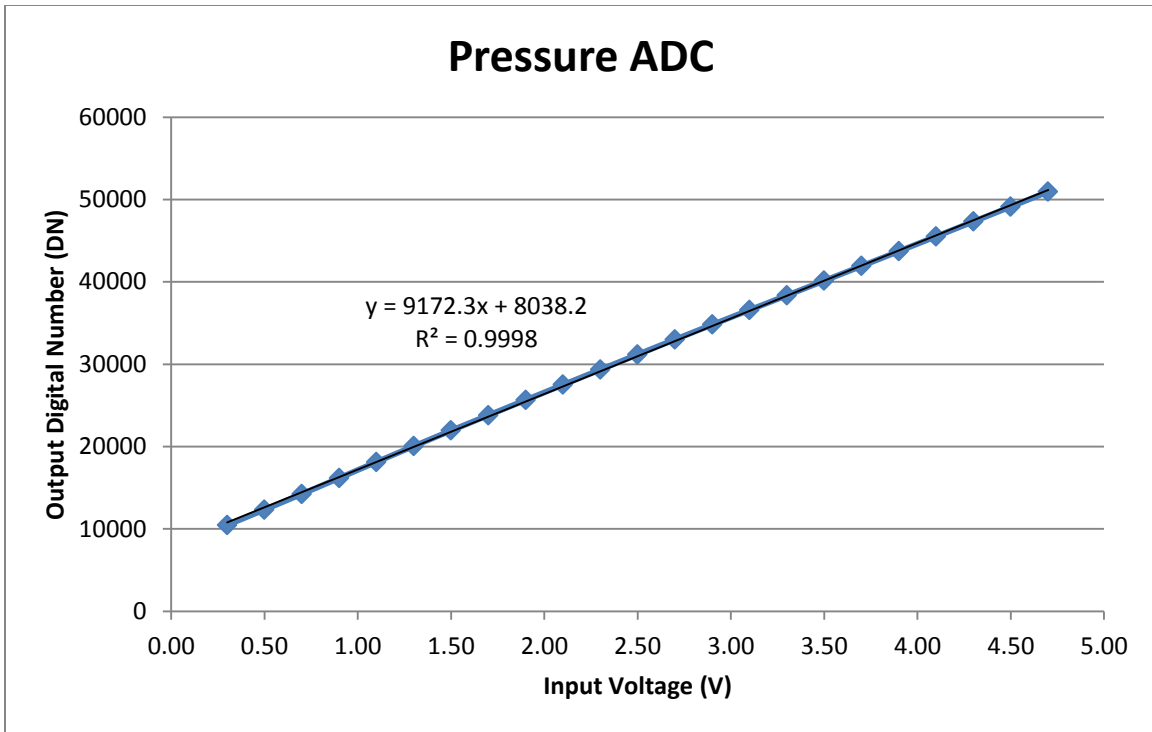
Fig. 14. Preliminary pressure ADC output DN vs input voltage.

The pressure ADC also shows great linearity at an r-squared value of 0.9998. This is consistent with the preliminary temperature ADC measurement. It is also apparent that the pressure measurement shows an opposite slope as the temperature ADC. This is because the pressure sensor outputs a voltage between 0.5 and 4.5 V. This voltage range is too large for the common mode input range of the ADC, so an inverting gain and shift operational amplifier was implemented to scale the 0.5 to 4.5 V range down to 1.8 to 3.2 V. This prevents the ADC from receiving voltage levels beyond its input common mode range and outputting invalid data. This scaling is done most easily with an inverting configuration. Thus the pressure signal conditioning and digitization show an inverted behavior with respect to the preliminary temperature ADC test (Fig. 8).

The system pressure calibration differs from the system temperature calibration and is expected to be highly linear. This is because the pressure sensor outputs a voltage controlled by internal feedback loop instead of a current; thus it is not dependent on temperature-sensitive output node impedance. The result of pressure calibration for all five systems is shown in Figs. 15 through 19. The blue data points represent sweeping the pressure input to the pressure sensor in 2.5 psi increments (Fig. 4).

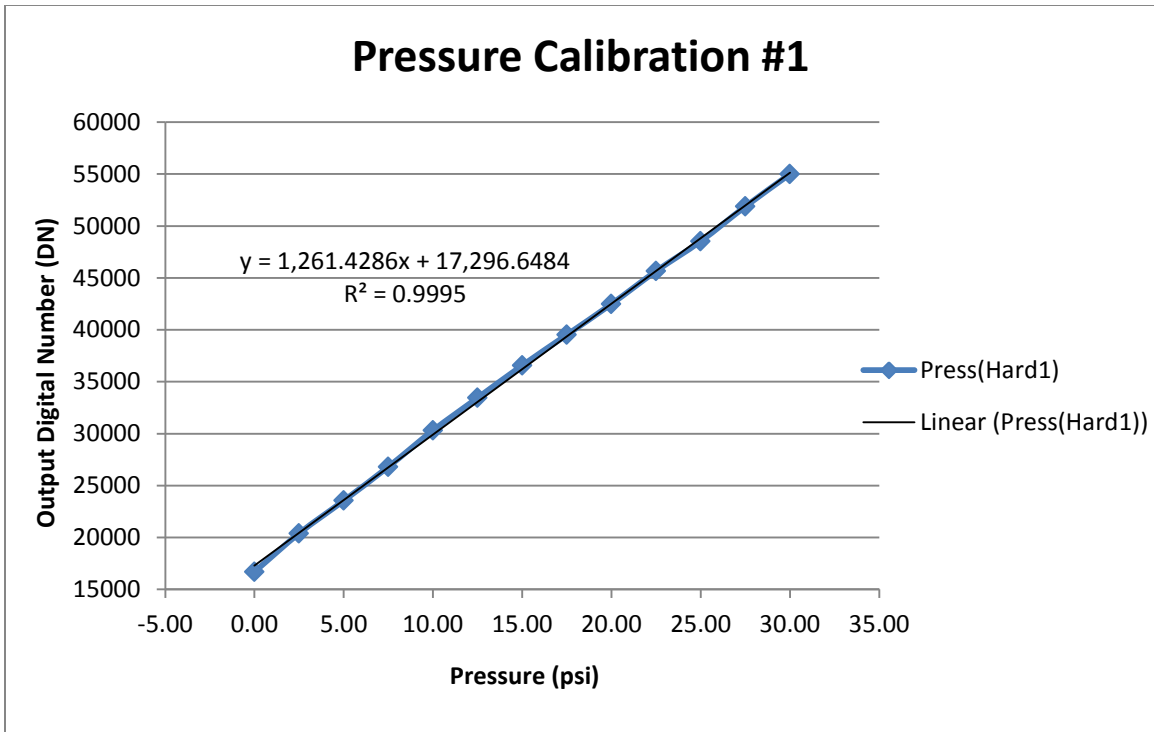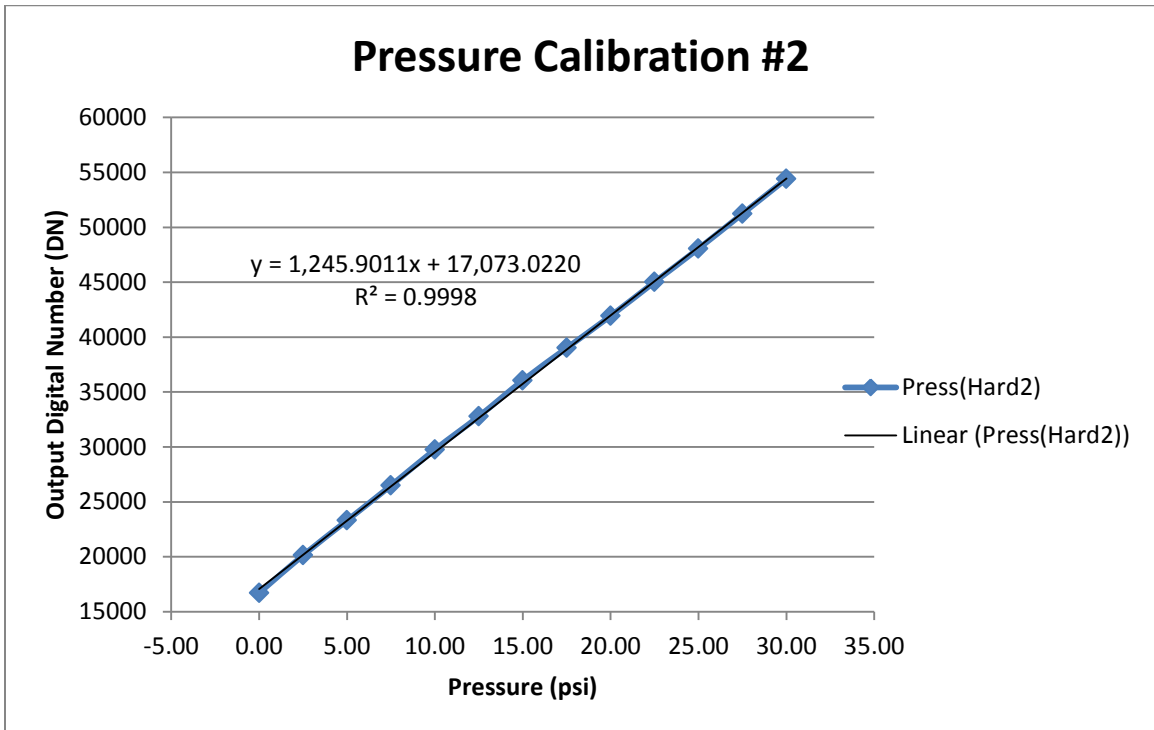**Fig. 15. System 1 pressure output DN vs ambient pressure.**

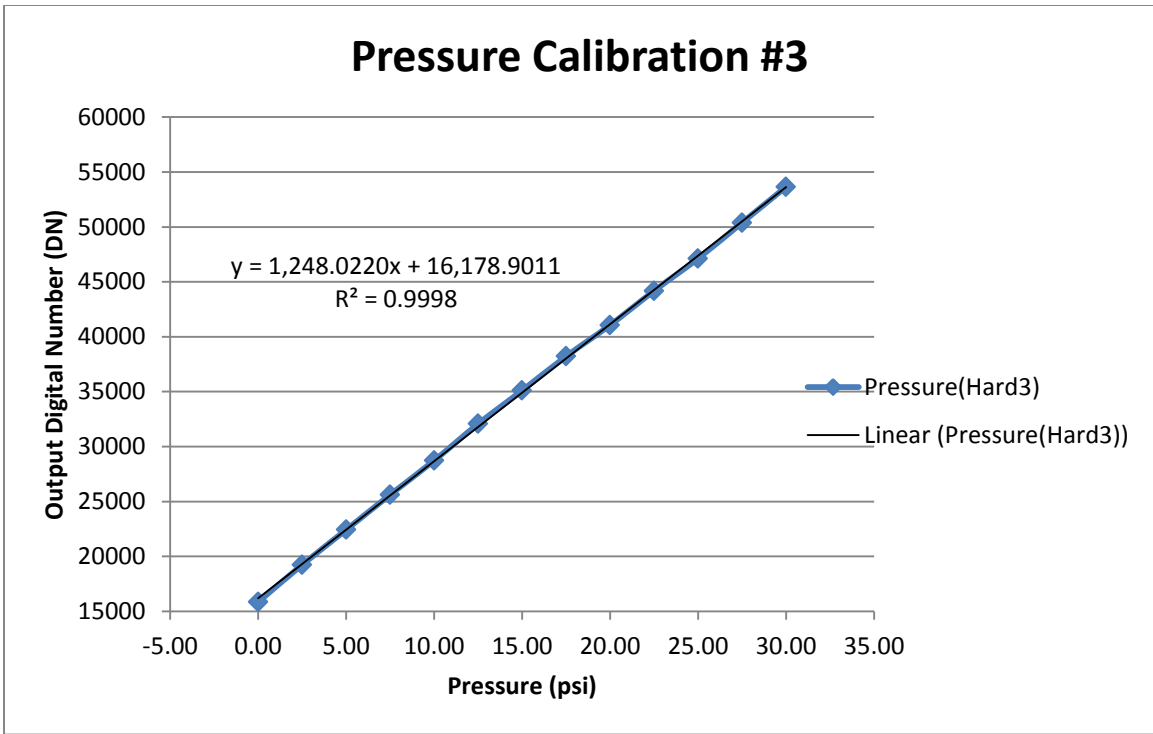**Fig. 16. System 2 pressure output DN vs ambient pressure.**

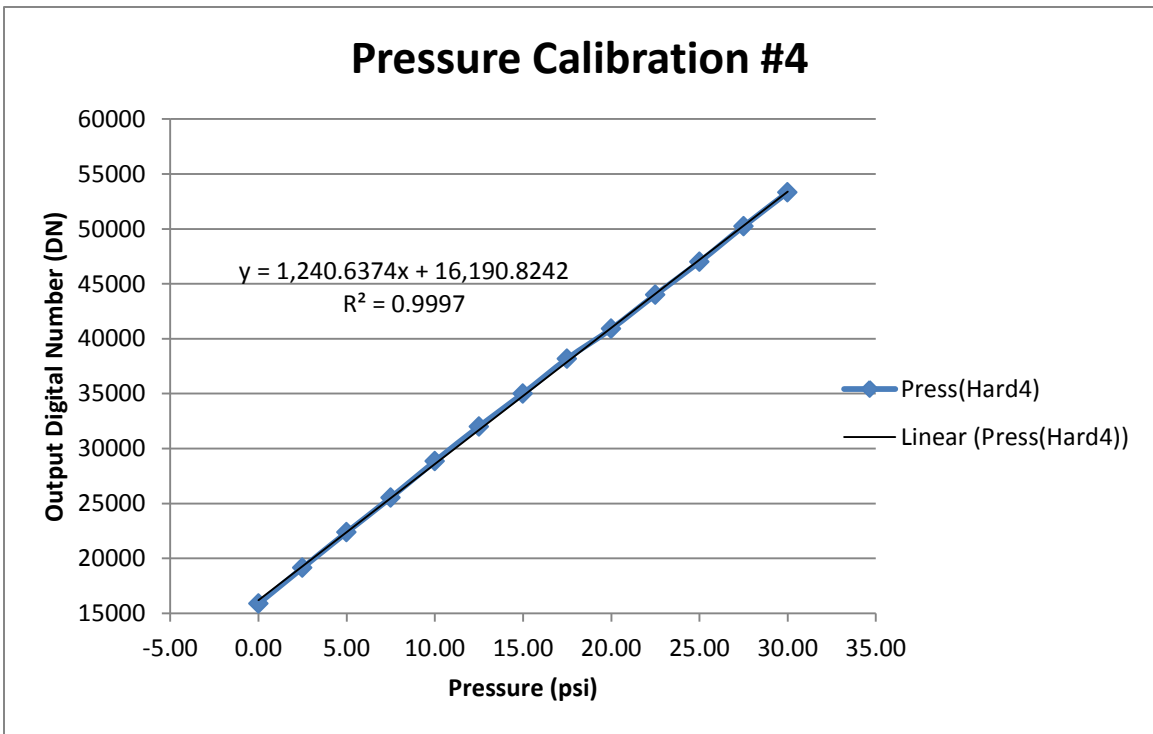**Fig. 17. System 3 pressure output DN vs ambient pressure.**

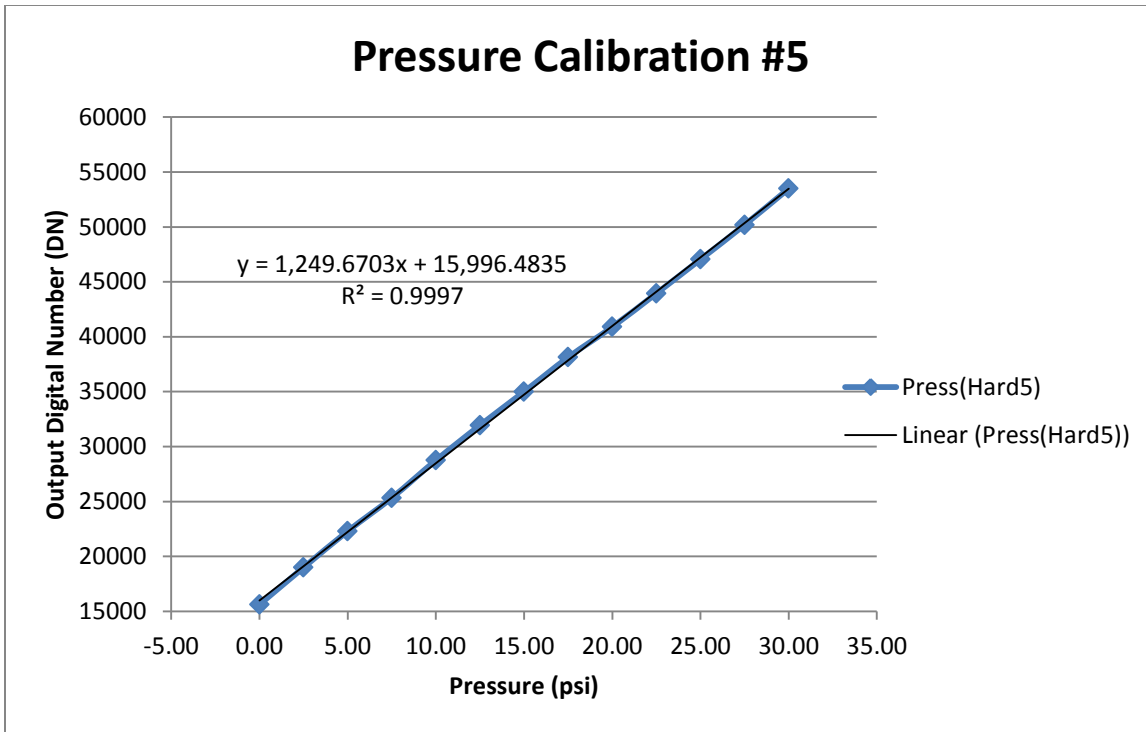**Fig. 18. System 4 pressure output DN vs ambient pressure.**

Fig. 19. System 5 pressure output DN vs ambient pressure.

The pressure calibration data for all five systems show great linearity. This result matches the expectations for the pressure sensor and validates the consistency and accuracy of both the pressure sensor and the rad-hard circuitry, making for a simple trendline approximation. A linear fit produces the best approximation for all five systems. Table 2 summarizes for each system the linear r-squared values and coefficients that are used by LabVIEW to convert output DNs to ambient data.

Table 2. Summary of system pressure calibrations fit values and coefficients

System	R-squared fit value	Coefficients (a, b)
1	0.9995	1261.429, 17296.65
2	0.9998	1245.901, 17073.02
3	0.9998	1248.022, 16178.90
4	0.9997	1240.637, 16190.82
5	0.9997	1249.670, 15996.48

3.3 GAMMA DETECTION CALIBRATION

The gamma detection calibration is different in nature from both the temperature and pressure calibrations, in that the charge generated by the event is only present for a short period of time, and it needs to be classified. The current spike output from the G-M tube is converted to voltage through a resistor and, depending on the peak level of current, the voltage will also reach a certain peak value. In order to discern whether a voltage spike is in fact a radiation event, a certain voltage threshold must be met. This can be achieved by comparing the voltage spike with a reference voltage that is unachievable by any excitation other than a radiation event. If the voltage spike surpasses the threshold, the comparator will output a digital "high value, representing one event, and subsequently will return to a digital low in

preparation for the next event. These events can be summed with an FPGA digitally implemented counter, which will notify users of the total ionizing dose as well as the dose rate, which is derived through the rate of change of the event count.

The first step in calibrating the gamma detection performance is optimizing the G-M tube output voltage amplitude for compatibility with the system. The comparator operates on a 5 V supply and could be damaged if voltage spikes larger than 5 V are present on its input. A potentiometer is used to scale the current-to-voltage conversion down to the necessary amplitude of about 4.5 V. This waveform was captured on an oscilloscope and is shown as the yellow spike in Fig. 20.

The next step is to ensure that the comparator exhibits sufficient rise and fall times to record every gamma event output from the G-M tube without overlap. Maximizing the gain bandwidth of the comparator through all available parameters will produce the fastest rise and fall times possible for a given comparator design. In this case, we have control over the input bias current, which was increased to a maximum 150 µA. The result is a 30 ns rise time, shown in Fig. 20 as the green waveform. The maximum event rate of the G-M tube is 50,000 cps, which is equivalent to 20 µs per count [3]. This means that the comparator needs to produce a digital high value and return to a digital low within 20 µs of the initial gamma event pulse. Figure 20 shows that the comparator easily achieves this requirement, with about a 600 ns pulse width and only about 800 ns until the output completely settles back to digital low. With these specifications, the comparator, assuming the voltage threshold reference is set properly, will capture every gamma event.
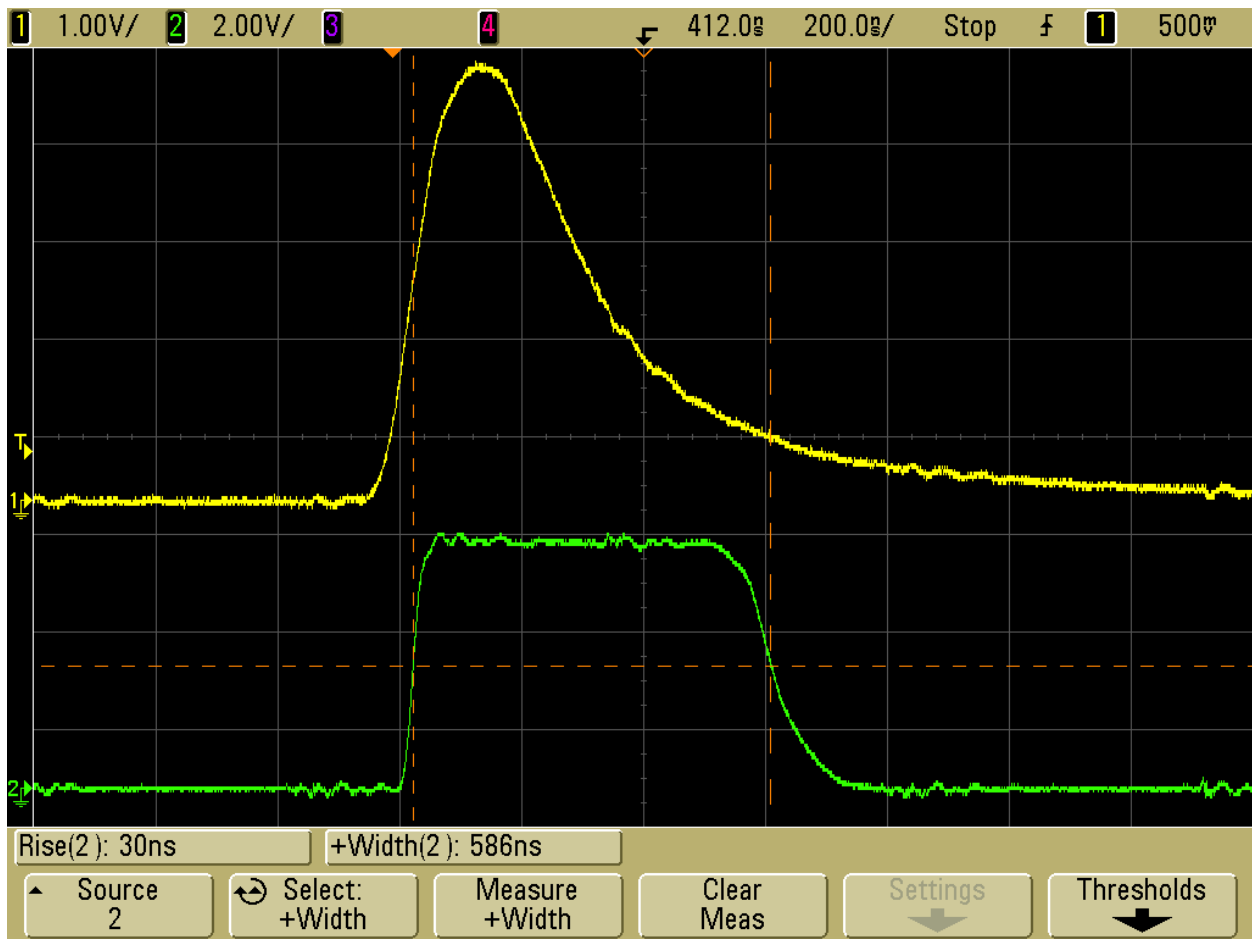

Fig. 20. Gamma event and comparator output pulse response.

The voltage threshold for the comparator must be optimized to allow classification of each gamma event but to reject any other voltage spikes (e.g., spikes that may be induced by noise or incident radiation). Because the G-M tube functions based on an avalanche effect and produces a large amount of charge, the potentiometer resistance must be set relatively low in order to achieve the 4.5 V pulse shown in Fig. 20. At such a low resistance, it is unlikely that any voltage spikes from charge deposition, other than those produced by the G-M tube, will result in a signal with an amplitude larger than 0.5 V. Thus the voltage threshold reference for the comparator can safely be set to 0.5 V to produce large enough pulse widths for the counter to recognize while also discarding any unwanted, spurious signals.

4. POSTIRRADIATION PERFORMANCE TESTING

For circuits that are unprotected against TID radiation, severe nonideal behavior can result as a function of increasing total radiation dose. These effects include shifts in device threshold voltages, increased leakage currents, and uncharacteristic extreme variation in circuit performance. In modern submicron processes, voltage threshold variations have been almost completely mitigated due to reduced gate oxide thickness and charge-trapping ability. However, leakage currents and performance variations still pose issues, and circuits designed for radiation hardness need to be verified against these effects.

Annular gate and guard ring layout techniques are popular methods for mitigating increased leakage currents and thus extreme performance variation. These techniques are featured in the Triad VCA and FMI frequency synthesizer ASICs used for analog-to-digital conversion on the rad-hard board. Consequently, the expectation for leakage current and system performance variations as a function of TID radiation is minimal. Although, as seen in the temperature calibration data, if any radiation chamber temperature change induces a shift in node resistance on the output of the temperature sensor, some slight nonlinear increase in data will be apparent. Significant increases in leakage current will manifest in system current consumption data since a large portion of the system's power expenditure is on the rad-hard board itself. It is also likely that severe leakage currents will induce changes in circuit quiescent points and will be apparent in the system performance data shown in Figs. 25 through -33.

For the purposes of radiation testing, three complete systems (systems 1, 4, and 5)underwent radiation exposure within the Gammacell 220. This is enough of a sample size to effectively analyze the radiation tolerance of the system while also preserving two systems (systems 2 and 3) for any future preradiation uses. System 5 was irradiated to a total dose of 200 kRad, and the remaining two systems, system 1 and 4, was irradiated to a total dose of 300 kRad. The project proposal [1] stated a requirement of only 200 kRad total dose exposure for each system, but typical radiation "tolerant" qualification for circuitry is at the threshold of 300 kRad total dose, and this qualification is useful for making claims about the system in conference or journal report submissions. Figure 21 shows an image of the rad-hard board inside the containment chamber before being lowered into the gamma radiation pool at test commencement.

Fig. 21. Rad-hard board setup before test commencement.

4.1 CURRENT CONSUMPTION RADIATION PERFORMANCE

The first parameter susceptible to radiation effects to consider is leakage current. Significant increases in device leakage current will produce large changes in the current consumption of the system. Therefore, values of system current consumption were recorded for all three irradiated systems every hour throughout the duration of the test. The recorded measurements for system 1 (Fig. 22) show a small dip in current consumption approaching the midpoint of the test and a slight increase during the latter portion of the test but not beyond the predose measurement value of 142.88 mA. System 4 measurements (Fig. 23) reveal only just resolvable variation throughout the duration of the test, beginning at 150.69 mA and ending at 151.28 mA. System 5 measurements (Fig. 24) depict a slow, consistent decrease in current consumption of about 13 µA/kRad until the 200 kRad stopping point. The maximum percent error from predose measurement for systems 1, 4, and 5 are 1.64%, 0.45%, and 1.71%, respectively. Not enough variation in current biasing has occurred to induce shifts in device quiescent points. All of these small

variations signify large amounts of excess charge being generated and escaping the circuit nodes by electric field through the power supply terminals but do not represent induced leakage current effects as a function of TID radiation. Moreover, at these levels of percent error, the radiation hardness of the exposed circuitry is proven with respect to radiation-induced leakage current.
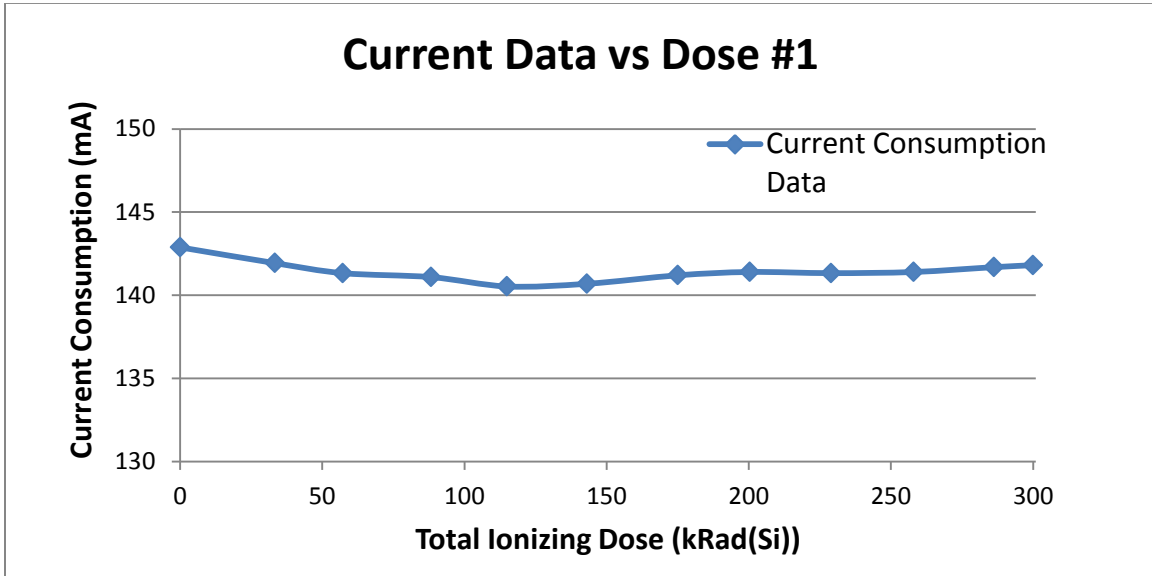

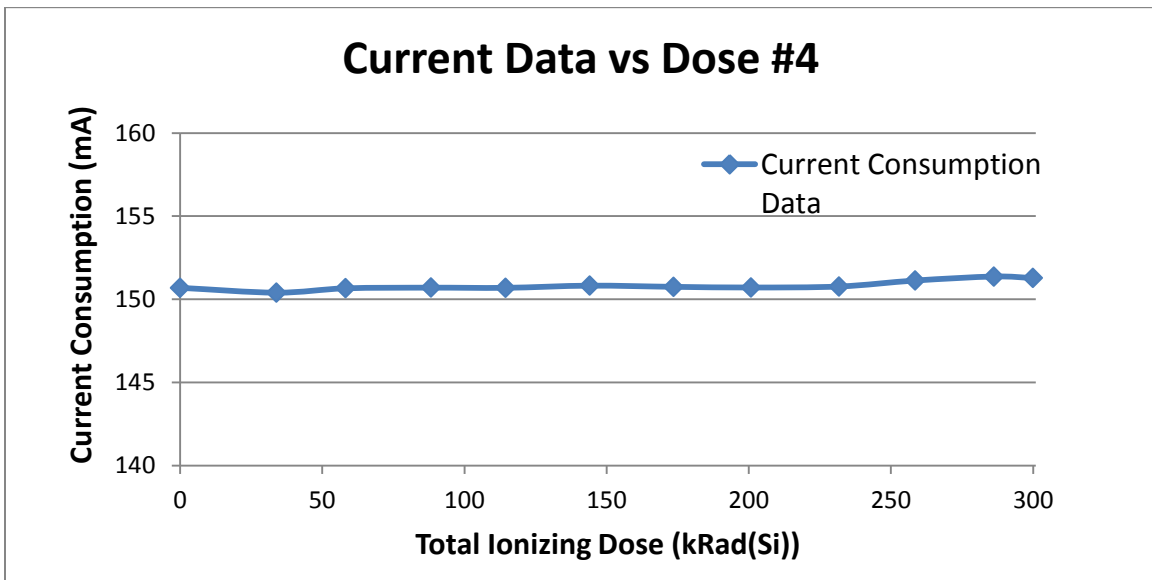**Fig. 22. System 1 current consumption vs TID radiation.**

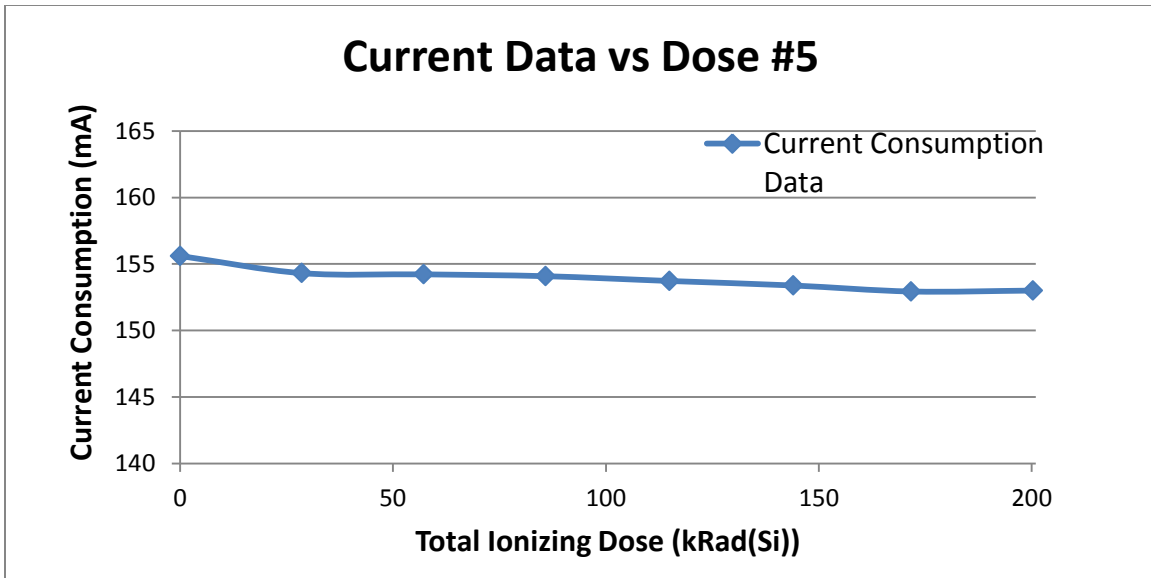**Fig. 23. System 4 current consumption vs TID radiation.**

Fig. 24. System 5 current consumption vs TID radiation.

4.2   TEMPERATURE DATA RADIATION PERFORMANCE

After leakage current effects are determined to not be a detriment to the performance of the data acquisition system, the actual ambient data output from the system needs to be examined as a function of radiation. The LabVIEW software recorded ambient temperature output data once every ten cycles. This was done to prevent excessive amounts of data from being taken but also to gather enough data for interpretations such as noise analysis to be performed. In addition, it is known that temperature sensors typically exhibit some initially unknown offset when compared to real temperature unless trimming is implemented using additional devices. The data are highly useful even without trimming because trends can be seen. During severe accident scenarios, trends are more important than actual temperatures.

The graphs of Figs. 25 through 27 relate the data acquisition system temperature data to ambient room temperature as a function of radiation. All three systems show a temperature data slope slightly more positive than the slope of the ambient room temperature. The larger slope of the temperature data is attributed to heating of the radiation chamber, in which radiation and heat from power dissipation in a small space are contributors, that induces inherent resistance shifts on the temperature sensor current output node, resulting in a voltage change. This is consistent with all three systems; even though the ambient temperature for system 5 was actually decreasing, system 5 also exhibits the least positive slope of all systems irradiated. The offsets of each sensor are also independently apparent, as two system's predose temperature data were below the room temperature, while the other system shows temperature data initially above the room temperature curve. By factoring out the effects of temperature sensor offset error and output node resistance temperature sensitivity, which are both due to the temperature sensor performance itself, the mask-programmable analog array can closely replicate ambient temperature data within a data acquisition system for nuclear reactor environment applications under extreme radiation conditions.
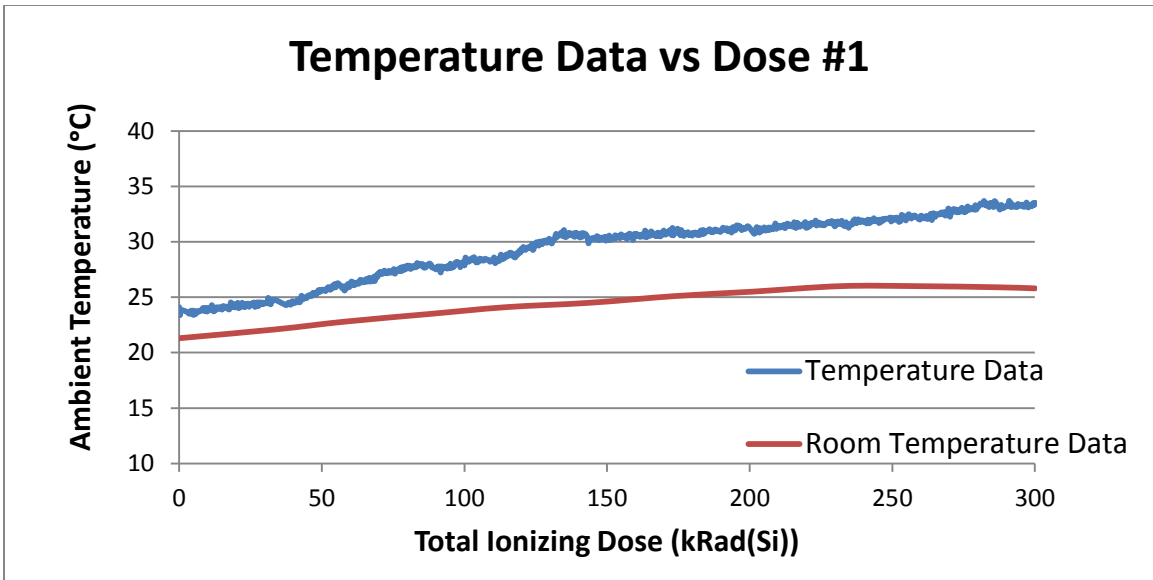
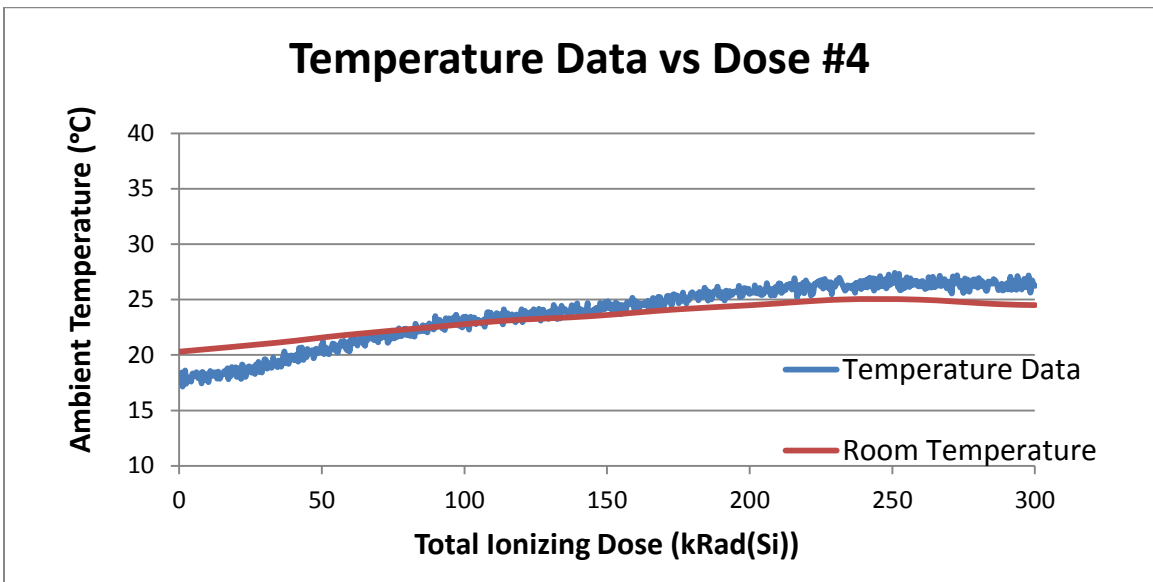**Fig. 25. System 1 temperature reading vs TID radiation.**

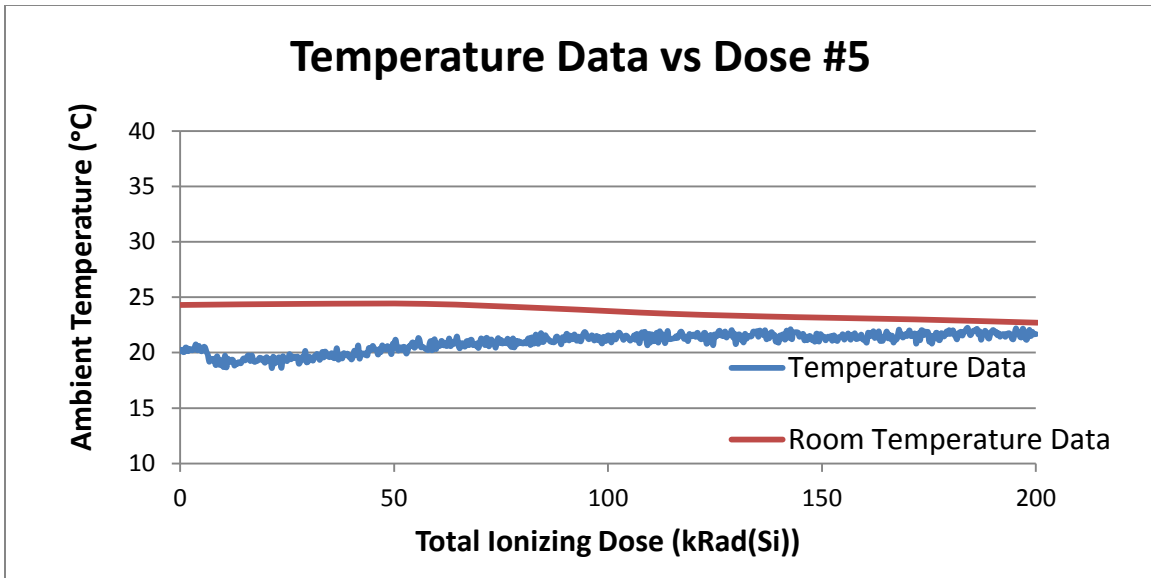**Fig. 26. System 4 temperature reading vs TID radiation.**

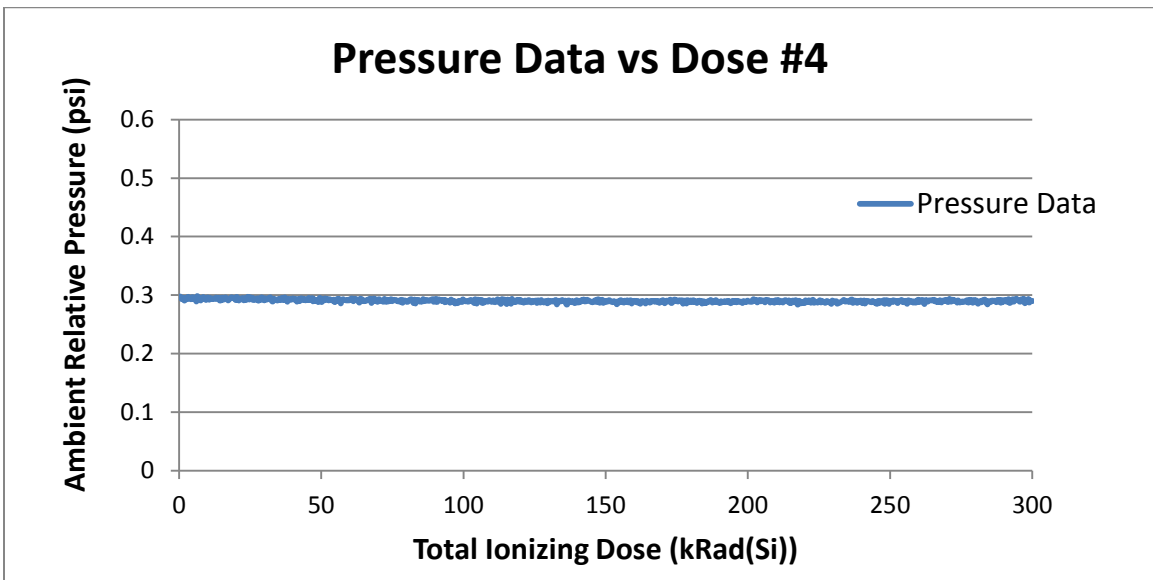**Fig. 27. System 5 temperature reading vs TID radiation.**

4.3 PRESSURE DATA RADIATION PERFORMANCE

As with the data acquisition system temperature radiation data, the LabVIEW software recorded ambient pressure output data once every ten cycles. Since the pressure sensor selected outputs a voltage that is closely controlled by an internal feedback loop and compensated against temperature and nonlinear effects, the output itself is not dependent on any other ambient parameter it will be exposed to, except pressure. This fact bodes well for the accuracy in performance of the data acquisition system pressure data as a function of radiation without the need to factor out any nonideal effects. The same sigma-delta modulator digitizes both the analog temperature and pressure data, so this improvement in sensor tolerance to atmospheric nonlinear effects should result in enhanced accuracy and stability relative to the temperature radiation data.

The graphs of Figs. 28 through 30 display the data acquisition system pressure data for systems 1, 4, and 5, respectively. All three systems show extremely consistent pressure data centered at about 0.3 psi, relative pressure. They also exhibit highly stable pressure data whose variation is only just visibly resolvable. The maximum percent error from predose measurements for systems 1, 4, and 5 are 4.51%, 2.66%, and 2.9%, respectively. A significant portion of that maximum percent error for each system is due to noise variations in the pressure data, although the pressure data noise is noticeably smaller in magnitude relative to the temperature data variations. Nonetheless, the pressure data exemplify the performance capabilities of the mask-programmable analog array in radiation-rich environments such as the data acquisition system for applications such as nuclear reactor environment monitoring as well as the improvement in authenticity of reported ambient data with the use of sensors qualified for specific implementations.
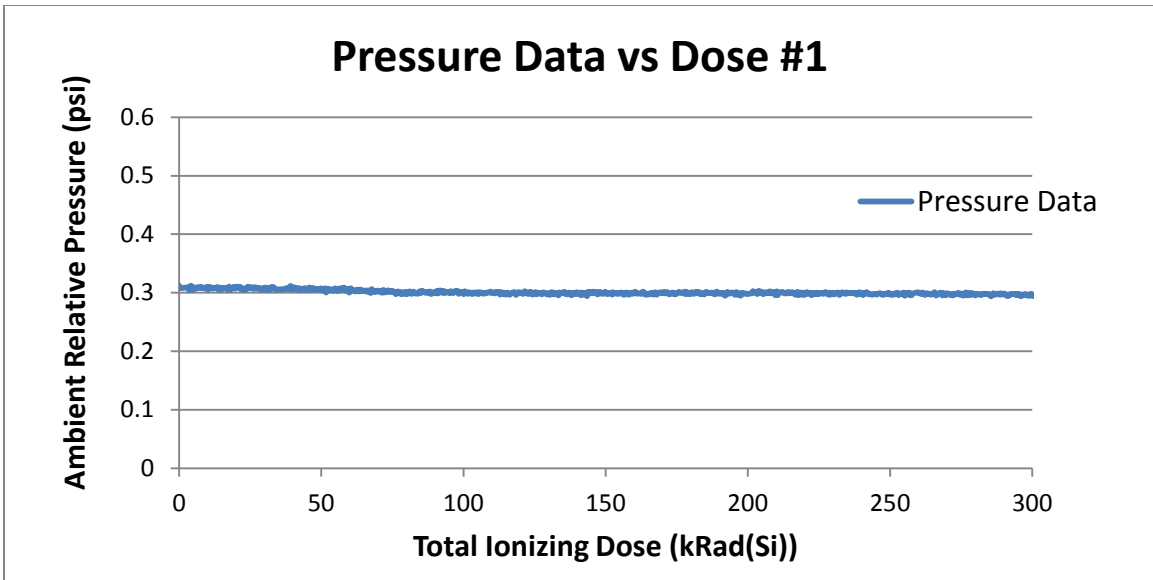
Fig. 28. System 1 pressure reading vs TID radiation.

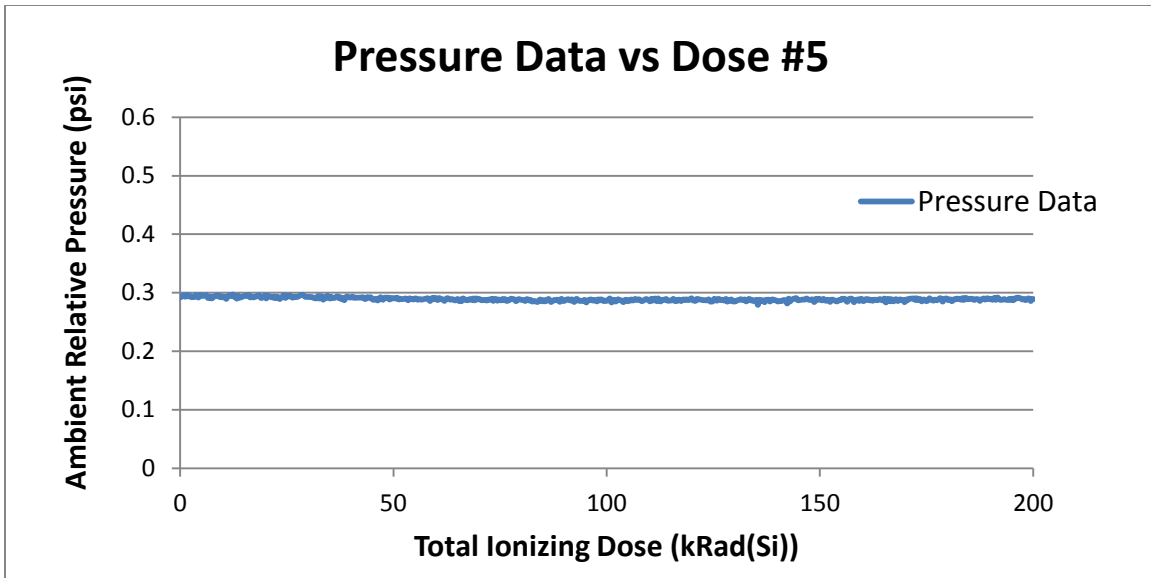**Fig. 29. System 4 pressure reading vs TID radiation.**

Fig. 30. System 5 pressure reading vs TID radiation.

4.4   GAMMA EVENT DATA RADIATION PERFORMANCE

The data gathering rate for gamma events was the same as that for the temperature and pressure parameters. The LabVIEW software recorded ambient pressure output data once every ten cycles. The G-M tube used for gamma radiation detection is capable of measuring up to 50,000 gamma counts per second, which saturates at roughly 400 Rad/h from cobalt-60. This rate is well above typical background radiation levels, so any significant count errors reported due to radiation exposure of the rad-hard electronics will be visible in the gamma event data. Since the gamma events are singular in nature and require digital electronics such as comparators and counters to be quantified, it is unlikely that TID radiation will induce populous bit count errors, but it is possible.

Normalized gamma events in units of counts per second were counted, calculated, and then plotted for systems 1, 4, and 5 in Figs. 31, 32, and 33, respectively. These plots show a seemingly random distribution of single gamma counts throughout the duration of the test. Nearly all of the relevant readings show about 0.3 cps, which equates to one gamma count in slightly less than a 4 s data gathering cycle. System 4 registered nothing higher than 0.3 cps during the entire duration of the test. System 5 reported two 0.6 cps cycles (two gamma counts slightly less than a 4 s cycle). System 1, in particular, shows a series of 0.6 cps cycles between the 100 kRad and 150 kRad TID radiation range. The data for system 1 are slightly peculiar but do not signify any count error due to radiation effects; an event rate of 0.6 cps still equates to background radiation levels, especially in a small laboratory containment housing multiple radiation sources. The data soon returned to the 0.3 cps standard level for these systems. Acquisition of these data concludes radiation tolerance testing for the data acquisition system, and the data confirm the ability of the mask-programmable analog array to condition and digitize analog signals accurately and efficiently in the presence of harsh radiation environments such as nuclear reactor containments.
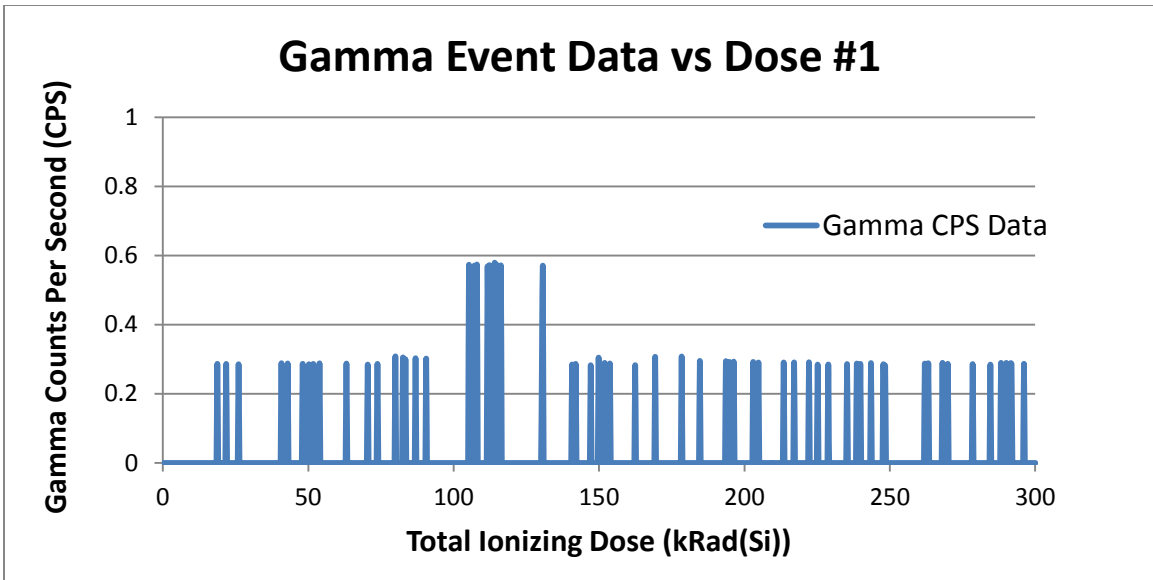
27

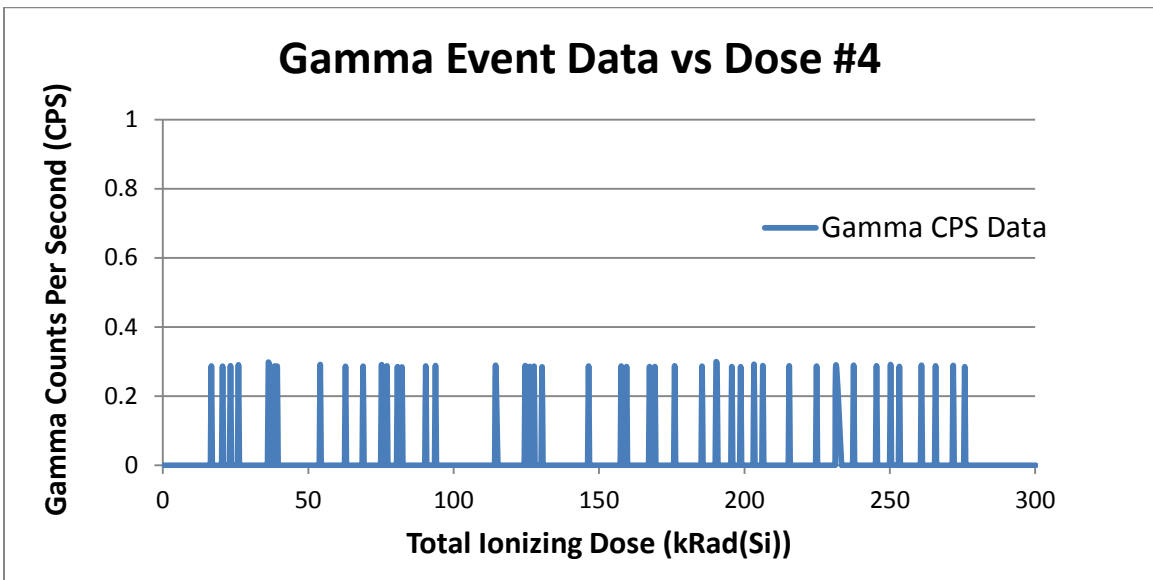**Fig. 31. System 1 gamma count rate vs TID radiation.**

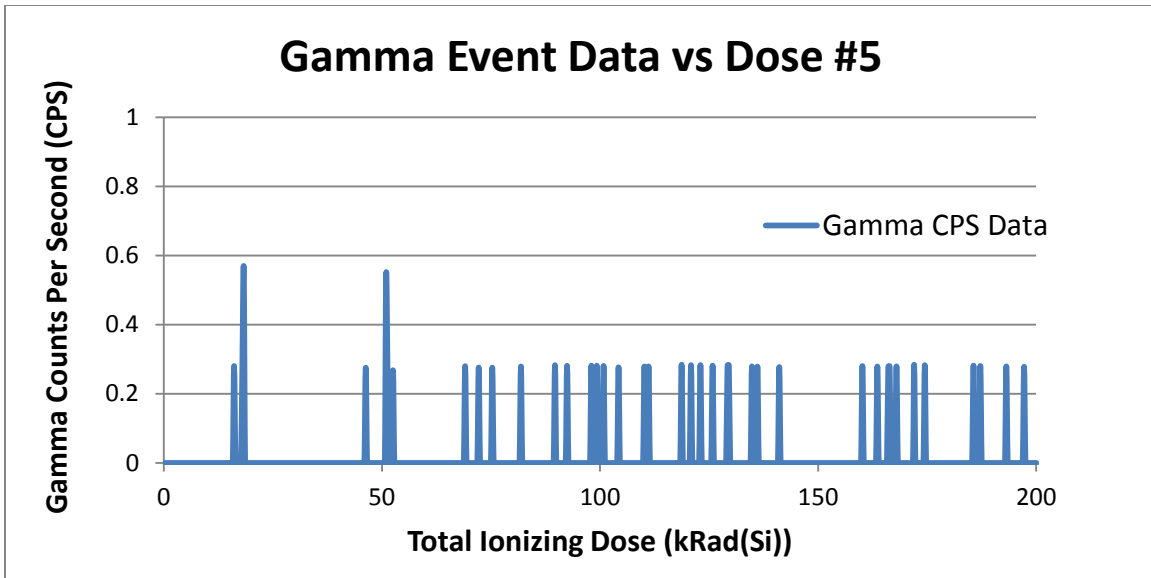**Fig. 32. System 4 gamma count rate vs TID radiation.**

Fig. 33. System 5 gamma count rate vs TID radiation.

5. CONCLUSION

We have presented the results of Task III of the NEET 2 project "Radiation Hardened Circuitry Using Mask-Programmable Analog Arrays" [1]. This task included complete system pre-irradiation calibration across pertinent temperature and pressure levels as well as performance validation as a function of TID radiation. LabVIEW software also was updated to allow for simplistic display of continuous time data that were converted from raw digital form using as-found calibration coefficients.

The testing and validation task was divided into two main phases, system calibration and radiation testing. The calibration phase was completed solely at Oak Ridge National Laboratory using on-site environmental temperature chambers, finely tunable pressure generators, and high-voltage equipment for the G-M tube output pulse. The radiation testing, using a cobalt-60 gamma source, took place at Arizona State University in a laboratory under the direction of Dr. Keith Holbert. Final detailed data analysis, qualification, and presentation will take place during Task IV of this NEET 2 project.

6. REFERENCES

1. C. L. Britton, M. N. Ericson, and B. Blalock, "Radiation Hardened Circuitry Using Mask-Programmable Analog Arrays," proposal submitted under NEET-2: Advanced Sensors and Instrumentation, 2012.

2. C. L. Britton et al., *Radiation Hardened Circuitry Using Mask-Programmable Analog Arrays*, Task II report submitted under NEET-2: Advanced Sensors and Instrumentation, September 2014.

3. C. L. Britton et al., *Radiation Hardened Circuitry Using Mask-Programmable Analog Arrays*, Task I report submitted under NEET-2: Advanced Sensors and Instrumentation, March 2014.

4. http://www.triadsemi.com/vca-technology/

5. http://www.frequencymanagement.com

APPENDIX A. LABVIEW INTERFACE SOFTWARE VISUAL CODE

CMD V2 Sub VI